Revealing the lipidome and proteome of *Arabidopsis thaliana* plasma membrane

Delphine Bahammou[1§], Ghislaine Recorbet[2§], Adiilah Mamode Cassim[2*], Franck Robert[2], Thierry Balliau[3], Pierre Van Delft[1], Youcef Haddad[1*], Arnaud Mounier[2], Sébastien Mongrand[1], Laetitia Fouillen[1#], Françoise Simon-Plas[2#]

1, Laboratoire de Biogenèse Membranaire, CNRS, Université. Bordeaux, (UMR 5200), F-33140 Villenave d'Ornon, France

2, UMR Agroécologie, INRAE, Institut Agro Dijon, Université Bourgogne Franche-Comté, F-21000 Dijon, France

3, Université Paris-Saclay, INRAE, CNRS, AgroParisTech, GQE-Le Moulon, PAPPSO, F-91190, Gif-Sur-Yvette, France

§ These two authors (DB and GR) contributed equally to the work, and should be considered as co-first authors

# These two authors (LF and FSP) contributed equally to the work, and should be considered as co-last authors

Corresponding author: Françoise Simon-Plas: francoise.simon-plas@inrae.fr

* current addresses:

AMC : Centre de Recherche INSERM LNC-UMR1231, 7 bd Jeanne d'Arc BP 87900, 21079 Dijon Cedex, France

YH : Institut de Génétique, Environnement et Protection des Plantes (IGEPP), UMR1349, INRAE-Institut Agro-Université de Rennes 1, domaine de la motte, 35653 Le Rheu Cedex, France

Conflicts of interest: none

Running title

Plant plasma membrane joint lipidome and proteome

Credit Author Statement

Delphine Bahammou, methodology, investigation, visualization, writing -review and editing

Ghislaine Recorbet, data curation, formal analysis, investigation, methodology, visualization, writing-original draft

Thierry Balliau, Adiilah Mamode Cassim, Franck Robert, Pierre Van Delft, Youcef Haddad: investigation, methodology, writing-review and editing

Arnaud Mounier, software, writing-review and editing

Laetitia Fouillen, Sébastien Mongrand: conceptualization, methodology, investigation, validation, visualization, writing-original draft

Françoise Simon-Plas, conceptualization, funding acquisition, project administration, validation, writing-original draft

Abbreviations

ARALIP (Arabidopsis acyl-lipid metabolism database)

ASG (acylated steryl glycoside)

Atμ (Arabidopsis microsomes)

AtPM (Aradidopsis plasma membrane)

BSTFA (*N*, *O*-bis(trimethylsilyl)trifluoroacetamide))

Cer (ceramide)

Col-0 (columbia-0)

DAG (diacylglycerol)

DGDG (digalactosyldiacylglycerol)

ER (endoplasmic reticulum)

FA (fatty acid)

FDR (false discovery rate),

G protein (guanine nucleotide-binding protein)

GIPC (glycosyl inositol phosphoryl ceramide)

GlcCer (glucosylceramide)

GO (gene ontology)

GPI (glycosylphosphatidylinositol)

GRAVY (grand average of hydropathicity index)

HDA (inferred from high throughput direct assay)

HP-TLC (high-performance thin layer chromatography)

hVLCFA (2-hydroxylated very long chain fatty acid)

ID (internal diameter)

IDA (inferred from direct assay)

LBD (lipid-binding domain)

LCB (long-chain base)

LCB-P (long-chain base-phosphate)

LC-MS/MS (liquid chromatography-tandem mass spectrometry)

LTP (lipid-transfer protein)

MCS (membrane contact site)

MGDG (monogalactosyldiacylglycerol)

MLP (multi-localizing protein)

MS (Murashige and Skoog)

MRM (multiple reaction monitoring)

NSAF (normalized spectral abundance factor)

PA (phosphatidic acid)

PASEF (parallel accumulation serial fragmentation)

PC (phosphatidylcholine

PE (phosphatidylethanolamine)

PG (phosphatidylglycerol)

PI (phosphatidylinositol)

PIP (phosphatidylinositol monophosphate)

PI4P (phosphatidylinositol 4-phosphate)

PIPT (phosphatidylinositol transfer protein)

PIP2 (phosphatidylinositol bisphosphate)

PM (plasma membrane),

PS (phosphatidylserine)

SG (sterylglycosides)

SP (N-terminal signal peptide)

SUBA (subcellular localization database for Arabidopsis proteins)

TIMS (trapped ion mobility spectrometry)

TM (trans-membrane)

VLCFA (very long chain fatty acid)

Abstract

The plant plasma membrane (PM) plays a key role in nutrition, cell homeostasis, perception of environmental signals, and set-up of appropriate adaptive responses. An exhaustive and quantitative description of the whole set of lipids and proteins constituting the PM is thus necessary to understand how its individual components, the way they are organized and interact together, allow to fulfill such essential physiological functions. Here we provide by state-of-the-art approaches the first combined reference of the plant PM lipidome and proteome from *Arabidopsis thaliana* suspension cell culture. We identified a core set of 2,165 proteins (406 of which had not been shown associated to PM previously), which is by far the largest set of available data concerning the plant PM proteome. Using the same samples, we combined lipidomic approaches, allowing the identification and quantification of an unprecedented repertoire of 405 molecular species of lipids. We showed that the different classes of lipids (sterols, phospholipids, and sphingolipids) were present in similar proportions in the plant PM. Within each lipid class, the precise amount of each lipid family and the relative proportion of each molecular species were then determined, allowing us to establish the complete lipidome of Arabidopsis PM, and highlighting specific characteristics of the different molecular species of lipids (for instance fatty acyl chain length and saturation according to the polar head). Results obtained are consistent with plant PM being an ordered mosaic of domains and point to a finely tuned adjustment of the molecular characteristics of lipids and proteins. More than a hundred proteins related to lipid metabolism, transport or signaling have been identified and put in perspective of the lipids with which they are associated. All these results provide an overall view of both the organization and the functioning of the PM.

Introduction

In all organisms, the plasma membrane (PM) forms a selective barrier between the cell and the extracellular environment and plays multiple roles, including homeostasis, regulation of nutritional status, signaling and stress response. The PM thus constitutes a sensor for modifications of cellular environment and a platform for intricate orchestration of signal transduction allowing translation of external signals in finely tuned appropriate adaptive responses. Throughout the different kingdoms, the PM of all living cells is made of a bilayer of lipids (with polar heads facing intra and extracellular medium) within which proteins are inserted (**1**). At the time this model of "fluid mosaic" was established, it was considered that lipids were mainly responsible of forming the hydrophobic barrier preventing the passive transfer of solutes and that proteins were responsible of all the active transport and signaling processes. If the fundamentals of this model have not been questioned, it has been tremendously enriched by the identification of additional elements concerning the organization and functioning of the PM (**2**).

A first element is the role of lipids as direct regulators of protein activity. Indeed, unlike bulk lipids, the lipid molecules in contact with an intrinsic membrane protein act as a solvent for the protein: these lipids have been referred to as boundary lipids or as annular lipids, to denote the fact that they form an annular shell of lipid around the protein (**3**, **4**.) Annular lipids have a slower dynamics than the bulk ones, and provide through their molecular characteristics (charge, steric hindrance of the polar head, length and unsaturation of the acyl chain) a well suited nano-environment for the surrounded intrinsic protein. Some membrane lipids might also act as cofactors directly regulating protein activity, these lipids often co-purifying with the protein and being resolved in high-resolution structures of the protein (**5**). The involvement of PIP_2 in the regulation of integral PM proteins has also emerged as a key process (**6**, **7**).

Membrane proteins are also quite sensitive to biophysical characteristics of the membrane which are fully dependent on its lipid composition. A typical feature of the membrane is the thickness of the hydrophobic core of the bilayer, which is expected to match the hydrophobic thickness of any protein embedded in the bilayer, since the cost of exposing either fatty acyl chains or hydrophobic amino

acids to water is very high (**8**). Any mismatch between the hydrophobic thickness of the lipid bilayer and the protein would lead to distortion of the lipid bilayer, or the protein, or both, to minimize it, as evidenced by the modulation of membrane protein structure and activity consecutive to changes in fatty acyl chain length (**9**, **10**). This points to a necessary fine adjustment between the length of protein TM helices and the thickness of the hydrophobic core of the lipid bilayer determined by the length of lipid acyl chains.

Another parameter to be considered as regulating membrane proteins is the viscosity combined with the lipid packing. Any molecule moving in a liquid environment experiences some frictional drag, opposing the movement. Such resistance to motion is expressed in terms of the viscosity or its inverse, fluidity (**11**). In a lipid bilayer, the resistance to motion will come predominantly from the lipid fatty acyl chains, the viscosity increasing with the average degree of saturation of the chains, as does the lipid packing (i.e.: the ability of lipids to stay tightly closed). Although the effects of membrane viscosity or lipid packing on the activities of membrane proteins are difficult to evidence, they have been involved in the regulation of the activity of some PM proteins (**12**, **13**). The lipid composition is also responsible for forces existing within membrane and also regulating membrane protein structure and activity. For instance, lipids, such as phosphatidylethanolamine, that prefer to adopt a curved, hexagonal HII phase (**14**) will favor a negative curvature generating tension in the corresponding zone of the membrane. The study of mechanosensitive channels provided insights on the mechanisms by which lipids convey mechanical stimuli causing membrane stretching or compression into an information perceived by proteins (**15**).

One of the major breakthroughs in the understanding of membrane organization since the description of the fluid mosaic model was the discovery that PM components are not homogeneously distributed within the membrane. The « lipid raft » hypothesis, bringing together structural and functional animal cell membrane organization thus proposed rafts as PM platforms of high molecular order (reflecting lipid packing), enriched in cholesterol and sphingolipids, in which proteins involved in signaling can selectively interact with effector molecules (**16**). Since an ever increasing number of proteins and lipids have been described as organized into nanometric membrane compartments, PM of living cells must now be acknowledged as a dynamic, highly compartmentalized mosaic wherein membrane

domains with different biophysical properties co-exist at different scales (**17**, **18**). The confining of membrane proteins in distinct nanodomains has been hypothesized as a way for plant cells to use similar proteins to respond differentially to various stimuli (**19**, **20**). This attractive hypothesis could be the first-stage physiological output of PM sub-compartmentalization, and in agreement with the membrane dynamics observed in the early steps of signal transduction (**21**, **22**). All studies performed either on artificial membranes, isolated biological membranes or PM of living cells demonstrated unambiguously that lipids were critical regulators of plant PM organization at a nanometer scale (**23**, **24**, **25**, **26**). Based on their tremendous structural diversity **(27**), plant lipids might account for the formation of plethora membrane domains (**28**).

Altogether, it is clear that the major physiological functions of PM fully rely on a finely tuned adjustment of its composition in lipids and proteins and on exquisitely spatially and timely regulated interactions of these components to deliver the right physiological outputs. Evidence has been recently provided that on the evolutionary scale, changes in membrane lipid composition may require adaptation of the membrane proteome (**29**). The most complete and accurate repertoire of the different molecular species of PM lipids and proteins is thus necessary to understand how they establish functional interactions to control PM organization and dynamics.

Different proteomes of purified plant PM have been characterized so far (for review see **30**, **31**, **32**) but the improvement of mass spectrometry methods prompted us to reembark on such approaches. Besides, although the lipids present in the PM of plants have already been analyzed in different species (**33**, **34**), an overall picture reporting the precise amount and molecular description of each lipid species in this membrane is still missing, particularly in the model plant Arabidopsis. Building a reference of the whole lipidome and proteome of plant PM from a single material seems all the more necessary that variations of molecular compositions from one species, or one organ, to another, make it very difficult to get a global picture from data collected in different studies. So far, the only joint description of PM lipidome and proteome, has been performed on *Mesembryanthemum crystallinum* focusing on changes triggered by salt stress (**35**). This paper reports the first joint extensive characterization of Arabidopsis PM (further called AtPM) lipidome and proteome using cell suspension as a starting material, using state of art methods. *Arabidopsis thaliana* is the model plant

acting as a reference for the plant biologist. Suspension cells were identified as a suitable starting material for several reasons: (i) they are cultivated in constant conditions (temperature, light, culture medium), and fully devoid of microbial contaminations, thus avoiding the risk of possible fluctuation in their composition triggered by biotic and abiotic stress (ii) their undifferentiated nature allows to avoid the compositional bias inherent in the study of differentiated tissues.

The combined use of classical and newly developed methods allowed an in depth qualitative and quantitative characterization of the PM full lipidome and the use of sate of art proteomics methods and the benefit of the very recently actualized data bases yielded an unprecedented repertoire of PM proteins. The analysis of these two data sets in relation to each other provides clues to understand how the molecular characteristics of lipids and proteins determine the functional organization of the membrane.

Experimental procedures

Cell culture, PM preparation and purity

Arabidopsis cells ecotype Columbia-0 (Col-0) were grown in liquid culture consisting of Murashige and Skoog (MS) medium pH 5.6, containing MS salts, Nitsch vitamins, α-naphthalene acetic acid (0.5 mg/L), kinetin (0.05 mg/L) and sucrose (30g/L). Cell multiplication was carried-out by weakly dilution (20:100) into fresh medium under continuous light, 25 °C, and shaking (150 rpm). Microsome and PM preparations were performed at 4 °C. Microsomal proteins were extracted using the differential centrifugation procedure described by Stanislas et al. (**36**). Cells were collected by filtration during the exponential phase, frozen in liquid nitrogen, and homogenized with a Waring Blendor in grinding medium (50 mM Tris-MES, pH 8.0, 500 mM sucrose, 20 mM EDTA, 10 mM DTT, and 1 mM PMSF). The homogenate was centrifuged at 16,000 X *g* for 20 min. After centrifugation, supernatants were collected, filtered through two successive screens (63 and 38 µm), and centrifuged at 96,000 X *g* for 35 min. The resulting microsomal fraction was purified by partitioning in an aqueous two-phase system (polyethylene glycol 3350/dextran T-500, 6.6% each) to obtain the PM fraction (**37**). The sensitivity of ATPase activity to vanadate was used as PM marker (**38**). This protocol was repeated three times in order to obtain three independent microsomal (Atµ)

preparations and three corresponding PM (AtPM) fractions. Protein and lipid profiling experiments were further performed on the latter PM fractions according to the workflow schematized in **Figure 1**.

Protein profiling

Sample pre-fractionation and protein digestion

For each biological replicate (n = 3) of Atμ and AtPM proteins (10 µg) were pre-fractionated by a 0.5 cm migration on 12% SDS-PAGE. After Coomassie Brillant Blue staining, each gel was washed in distilled water, destained using 100 mM NH_4CO_3 in 50% acetonitrile, and then cut into 3-mm squares for subsequent proteomic analysis. A reduction step was performed by addition of 40 µl of 10 mM dithiotreitol in 50 mM NH_4HCO_3 for 30 min at 56 °C. The proteins were alkylated by adding 30 µl of 55 mM iodoacetamide in 50 mM NH_4HCO_3 and allowed to react in the dark at room temperature for 45 min. Gel pieces were washed in 50 mM NH_4HCO_3, then ACN, and finally dried for 30 min. In-gel digestion was subsequently performed for 7 h at 37 °C with 125 ng of modified trypsin (Promega) dissolved in 50mM NH_4CO_3. Peptides were extracted successively with 0.5% (v/v) TFA and 50% (v/v) ACN and then with pure ACN. Peptide extracts were dried and suspended in 25 µl of 0.1% (v/v) HCOOH, and 2% (v/v) ACN.

Liquid chromatography-tandem mass spectrometry (LC-MS/MS) analysis

Peptide separation was performed using a nanoelute UHPLC (Bruker, BillerikaUSA). Peptides were first desalted using a nanoEase Symmetry C18 TrapColumn, (100Å, 5 µm, 180 µm X 20 mm, Waters) with 0.1% HCOOH (v/v) in water for 1 min at 100 bar. Peptides were further separated on a Aurora C18 column (25 cm × 75 µm ID, 1.6 µm FSC C18, ionOptics). The mobile phase consisted of a gradient of solvents A: 0.1% HCOOH (v/v), in water and B: 100% ACN (v/v), 0.1% HCOOH (v/v) in water. Separation was set at a flow rate of 0.3 µl/min using a linear gradient of solvent B from 2 to15% in 60 min, followed by an increase to 25% in 30 min, 37% in 10 min, 90% in 5 min and finally to 90% for 10 min. Eluted peptides were analyzed with a timsTOF Pro (Bruker) using a Captive spray interface. Ionization (2 kV ionization potential) was performed with a liquid junction. Peptide ions were analyzed using Bruker otofControl 6.2.0 on PASEF Mode with tims activated, a m/z range from

100 to 1700, and a mobility ramp from 0.60 Vs/cm² to 1.6 Vs/cm². Each acquisition cycle was performed with 1 MS of 100ms, followed by 10 PASEF frames of 100 ms. For each PASEF frame, 10 MS/MS spectra were acquired with a rolling collision energy from 20eV to 59eV. Isolation was set at 2m/z for precursor mass less than 700 m/z and 3m/z for others. A dynamic exclusion was performed at 0.4min. Precursor was re-analyzed when intensity was 4 times higher than the previous scan to achieve a global MS/MS spectrum intensity of 20K counts.

Protein identification

Proteins were identified using X!Tandem (version 2015.04.01.1) (**39**) by matching peptides against the Araport11 database (www.araport.org) containing 48,358 protein entries downloaded from (https://www.araport.org/downloads/Araport11_Release_201606). Enzymatic cleavage was declared as a trypsin digestion with one possible missed cleavage in first pass. Cysteine carbamidomethylation were set to static, while methionine, protein N-terminal acetylation with or without excision of methionine, dehydration of N-terminal glutamic acid, deamination of N-terminal glutamine and N-terminal carbamidomethyl-cysteine as possible modifications. Precursor mass precision was set to 10 ppm with a fragment mass tolerance of 0.5 Da. Identified proteins were filtered and grouped using X!TandemPipeline (**40**) according to (i) the tolerated presence of at least two peptides with an *E*-value smaller than 0.01 and (ii) a protein *E*-value (calculated as the product of unique peptide *E*-values) smaller than 10^{-5}. These criteria led to a false discovery rate (FDR) of 0.3% for peptide and protein identification.

Experimental design and statistical rationale

Protein abundance values were calculated by spectral counting using normalized spectral abundance factor (NSAF) analysis that is based on the cumulative sum of recorded peptide spectra matching to a given protein (**41**). This method estimates protein abundance by first dividing the spectral count for each protein by the protein length and then dividing this number by the sum of all length normalized spectral counts for each organism and multiplying by 100. A NSAF value was calculated for each protein across the six replicates (three biological replicates for each microsomal and PM preparations). As NSAF represent percentages all data, when necessary for statistical analysis, were arcsine square

root-transformed to obtain a distribution of values that could be checked for normality using the Kolmogorov-Smirnov test. Significant (p-value < 0.05) differences between transformed NSAF values were analyzed using the Welch-test (degrees of freedom = n−1), which is compatible with unequal variances between groups (**42**).

In silico protein characterization

Digital immunoblotting that refers to the MS-based quantification of proteins having an exclusive cellular component localization (**43**), was performed by combining experimentally know localization with NSAF spectral counting. Experimentally known localization of proteins, as inferred from HDA (Inferred from High Throughput Direct Assay) and IDA (Inferred from Direct Assay) GO experimental evidence codes for cellular components (http://geneontology.org), was searched against Araport11 (https://www.arabidopsis.org/) (**44**) and SUBA5 (https://suba.live/) (**45**) built on the TAIR10 Arabidopsis proteome.

Alpha-helical trans-membrane (TM) regions and length were predicted according to TMHMM-2.0 (https://services.healthtech.dtu.dk/service.php?TMHMM-2.0). The presence of N-terminal signal sequences (SPs) that drive protein translocation across or integration to membranes, was predicted according to SignalP 5.0 (https://services.healthtech.dtu.dk/service.php?SignalP-5.0). The GPS-Lipid server (http://lipid.biocuckoo.org/webserver.php) was used as the lipid modification predictor for N-myristoylation, S-palmitoylation, and prenylation (S-farnesylation and/or S-geranylation. Glycosylphosphatidylinositol (GPI) anchor (i.e. glypiation) prediction was performed using NetGPI-1.1 (https://services.healthtech.dtu.dk/service.php?NetGPI-1.1). GRAVY values for protein sequences, defined by the sum of hydropathy values of all amino acids divided by the protein length, were retrieved using the GRAVY calculator (https://www.gravy-calculator.de/). Isoelectric points (pI) were retrieved from SUBA5. Protein localization predictions refer to non-HDA/non-IDA codes searched against Araport11 together with SUBA5 annotations, which include SUBA consensus and SUBA all predictors. The function of the identified proteins was sought using the Mercator 3.6 web-based pipeline (https://plabipd.de/), which divides proteins into 35 hierarchical, non-redundant functional classes using MapMan bin codes (**46**). Arabidopsis Acyl-Lipid Metabolism Database (ARALIP:

http://aralip.plantbiology.msu.edu/; **47**), and Uniprot (https://www.uniprot.org/) were also used for annotation of lipid-related proteins.

Lipid profiling

Absolute quantification of lipid moieties by GC-MS

For the analysis of total fatty acids by GC-MS, 200µg of AtPM was transmethylated at 110 °C overnight in methanol containing 5% (v/v) sulfuric acid and spiked with 10 µg of heptadecanoic acid (C17:0) and 10 µg of 2- hydroxy-tetradecanoic acid (h14:0) as internal standards. After cooling, 3 mL of NaCl (2.5%, w/v) was added, and the released fatty acyl chains were extracted in hexane. Extracts were washed with 3 mL of saline solution (200 mM NaCl and 200 mM Tris, pH 8), dried under a gentle stream of nitrogen, and dissolved in 150 mL of BSTFA -trimethylchlorosilane. Free hydroxyl groups were derivatized at 110 °C for 30min, surplus BSTFA-trimethylchlorosilane was evaporated under nitrogen, and samples were dissolved in hexane for analysis using GC-MS.

For the analysis of sterols moieties by GC-MS, 200µg of AtPM was transmethylated at 85 °C, for a shorter time to avoid degradation of sterols, i.e. 3h in methanol containing 1% (v/v) sulfuric acid spiked with 10µg of cholestanol, as internal standard. After cooling, 3 mL of NaCl (2.5%, w/v) was added, and the released sterol moieties were extracted in hexane. Extracts were washed with 3 mL of saline solution (200 mM NaCl and 200 mM Tris HCl, pH 8), dried under a gentle stream of nitrogen, and dissolved in 150 mL of BSTFA trimethylchlorosilane. Free hydroxyl groups were derivatized at 120 °C for 30min, surplus BSTFA-trimethylchlorosilane was evaporated under nitrogen, and samples were dissolved in hexane for analysis using GC-MS.

GC-MS was performed using an Agilent 7890A gas chromatograph coupled MS detector MSD 5975-EI (Agilent). An appropriate capillary column was used with helium carrier gas at 2 mL/min; injection was done in splitless mode; injector and mass spectrometry detector temperatures were set to 250 °C. Injection (1µl) was done in splitless mode; injector and mass spectrometry detector temperatures were set to 250 °C. Ionization energy was set at 70eV with m/z ranging from 40 to 700. For LCFA, HP-

5MS capillary column (5% phenyl-methyl-siloxane, 30-m, 250-mm, and 0.25-mm film thickness; Agilent) was used. The oven temperature was held at 50 °C for 1 min, then programmed with a 25 °C/min ramp to 150 °C (2-min hold) and a 10 °C/min ramp to 320 °C (6-min hold). For VLCFA, DB-23 capillary column (60-m, 250-mm, and 0.25-mm film thickness; Agilent) was used and the oven temperature was held at 50 °C for 1 min, then programmed with a 25 °C/min ramp to 210 °C (1-min hold) and a 10° C/min ramp to 306 °C and a 65 ° C/min ramp to 320 °C (3-min hold). For sterols moieties, HP-5MS capillary column (5% phenyl-methyl-siloxane, 30-m, 250-mm, and 0.25-mm film thickness; Agilent) was used and the oven temperature was held at 200 °C for 1 min, then programmed with a 10 °C/min ramp to 305 °C (2.5-min hold) and a 15 °C/min ramp to 320 °C. Quantification of sterols moieties and fatty acid methyl esters was based on peak areas, which were derived from total ion current, using the respective internal standards.

Biphasic extraction for sterol and glycerolipids analysis

200 µg of PM were used for TLC coupled with GC-MS analysis and 20 µg for LC-MS. Sample were extracted with chloroform:methanol (2:1, v/v) at room temperature. Polar contaminants such as proteins or nucleic acid were removed by adding 1 volume of 2.5% NaCl solution. After phase separation, the lower organic phase, which contains lipids, was harvested and the solvent was evaporated under a gentle flow of N_2 gas.

Monophasic extraction for sphingolipids

Sphingolipids were extracted from AtPM in the inferior phase of isopropanol/hexane/water (55:20:25, v/v) at 60 °C for 1h according to Toledo et al. (**48**). The extract was dried and resuspended in chloroform/methanol/water 30/60/8, v/v.

TLC Analysis of glycerolipids and and GlcCer

High-performance thin-layer chromatography (HP-TLC) plates were Silicagel 60 F254 (Merck, Rahway, NJ). Lipid extracts were chromatographed in chloroform:methanol:isopropanol:KCl 0,25%:methylacetate:triethylamine (30:10:25:7.8:24.3, v/v). Lipids were located under UV after

staining with primuline in acetone/water 80/20. Lipid bands were recovered from HPTLC plates and submitted to the acid hydrolysis and the GC-MS analysis, as described below.

TLC analysis of sterols

Sterol are extracted following the biphasic extraction, as described. High-performance thin-layer chromatography (HP-TLC) plates were Silicagel 60 F254 (Merck, Rahway, NJ). Extract lipids were chromatographed in chloroform:methanol (6:1, v/v). Lipids were located under UV after staining with primuline in acetone:water (80:20 v/v). Lipid bands were recovered from HP-TLC plates and submitted to the acid hydrolysis and the GC-MS analysis, as described below.

LC-MS/MS analysis of phospholipids

For the analysis of phospholipids by LC-MS/MS, lipid extracts were dissolved in 100 µL of solvent A (methanol/water 6/4 (v/v) + 10 mM ammonium formate +0.1%HCOOH) containing synthetic internal lipid standards (PE 17:0/17:0, PI 17:0/14:1 and PC 17:0/14:1 from Avanti Polar Lipids). LC-MS/MS (multiple reaction monitoring mode) analyses were performed with a model QTRAP 6500 (ABSciex) mass spectrometer coupled to a liquid chromatography system (1290 Infinity II, Agilent). Analyses were performed in the negative (PE, PG, PI) and positive (PC) modes with fast polarity switching (50 ms). Mass spectrometry instrument parameters were as follows: Turbo V source temperature (TEM) was set at 400 °C; curtain gas (CUR) was nitrogen set at 30 psi; the nebulizing gas (GS1) was nitrogen set at 40 psi; the drying gas (GS2) was nitrogen set at 50 psi and the ion spray voltage (IS) was set at -4500 or +5500 V; the declustering potential was adjusted between -160 and -85 V or set at +35V. The collision gas was also nitrogen; collision energy varied from -48 to -62 eV and +37 eV on a compound-dependent basis. MRM Transition are presented in **Supplemental Table S1**. Reverse-phase separations were performed at 40 °C on a Supercolsil ABZ plus 2.1x100 mm column with 120-Å pore size and 3-µm particles (Supelco). The gradient elution program was as follows: 0 min, 20% B (isopropanol/methanol 8/2 (v/v) + 10mM ammonium formate + 0.1% HCOOH); 10 min, 50% B; 54 min, 85% B. The flow rate was set at 0.20 mL/min, and 5mL sample volumes were injected. The areas

of LC peaks were determined using MultiQuant software (version 2.1; ABSciex) for relative phospholipid quantification.

LC-MS/MS analysis of sphingolipids

For the analysis of sphingolipids by LC-MS/MS, lipids extracts were then incubated 1h at 50 °C in 2 mL of methylamine solution (7ml methylamine 33% (w/v) in EtOH combined with 3mL of methylamine 40% (w/v) in water (Sigma Aldrich) in order to remove phospholipids. After incubation, methylamine solutions were dried at 40 °C under a stream of air. Finally, they were resuspended into 100 µL of THF/MeOH/H_2O (40:20:40, v/v), 0.1% HCOOH containing synthetic internal lipid standards (Cer d18:1/h17:0, Cer d18:1/C17:0, GlcCer d18:1/C12:0) was added, thoroughly vortexed, incubated at 60 °C for 20min, sonicated 2min and transferred into LC vials.

LC-MS/MS (multiple reaction monitoring mode) analyses were performed with a model QTRAP 6500 (ABSciex) mass spectrometer coupled to a liquid chromatography system (1290 Infinity II, Agilent). Analyses were performed in the positive mode. Nitrogen was used for the curtain gas (set to 30), gas 1 (set to 30), and gas 2 (set to 10). Needle voltage was at +5500 V with needle heating at 400 °C; the declustering potential was adjusted between +10 and +40 V. The collision gas was also nitrogen; collision energy varied from +15 to +60 eV on a compound-dependent basis. MRM transition are presented in **Supplemental Table S1**. Reverse-phase separations were performed at 40 °C on a Supercolsil ABZ+, 100x2.1 mm column and 5µm particles (Supelco).The mobile phase consisted of a gradient of solvents A: THF/ACN/5 mM ammonium formate (3/2/5 v/v/v) with 0.1% HCOOH and B:THF/ACN/5 mM ammonium formate (7/2/1 v/v/v) with 0.1% HCOOH. The gradient elution program for Cer and GlcCer quantification was as follows: 0 to 1 min, 1% B; 40 min, 80% B; and 40 to 42, 80% B. The gradient elution program for GIPC quantification was as follows: 0 to 1 min, 15% B; 31 min, 45% B; 47.5 min, 70% B; and 47.5 to 49, 70% B. The flow rate was set at 0.2 mL/min, and 5mL sample volumes were injected. For quantification the areas of LC peaks were determined using MultiQuant software (version 3.0; Sciex).

LC-MS/MS analysis of anionic phospholipids

725 µL of a MeOH/$CHCl_3$/1M HCl (2/1/0.1 v/v/v) solution and 150 µL water were added to the samples. Following the addition of the internal standard when appropriate and of 750 µL $CHCl_3$ and 170 µL HCl 2M, the samples were vortexed and centrifuged (1500 X *g*, 5 min). The lower phase was washed with 708 µL of the upper phase of a mix of MeOH/$CHCl_3$/0.01M HCl (1/2/0.75 v/v/v). Samples were vortexed and centrifuged (1500 X *g* / 3 min) and the washing was repeated once. Then, samples were kept overnight at -20 °C.

The organic phase was transferred to a new Eppendorf and the methylation reaction was carried out. For this purpose, 50 µL of TMS-diazomethane (2M in hexane) were added to each sample. After 10 min, the reaction was stopped by adding 6 µL of glacial acetic acid. 700 µL of the upper phase of a mix of MeOH/$CHCl_3$/H_2O (1/2/0.75 v/v/v) was added to each sample which was then vortexed and centrifuged (1500 x *g*, 3 min). The upper phase was removed and the washing step was repeated once. Finally, the lower organic phases were transferred to new Eppendorf. Following the addition of 100 µL MeOH/H2O (9:1 v/v), the samples were concentrated under a gentle flow of air until only a drop remained. 80 µL of methanol were added to the samples, which were submitted to ultrasounds for 1 minute, before adding 20 µL water, and be submitted to 1 more-minute ultrasound. The samples were finally transferred to HPLC vials for analysis.

Analysis of methylated anionic phospholipids (**49**) were performed using a liquid chromatography system (1290 Infinity II, Agilent) coupled to a QTRAP 6500 mass spectrometer (ABSciex). The chromatographic separation of anionic phospholipid species was performed on a reverse phase C18 column (SUPELCOSIL ABZ PLUS; 10 cm x 2.1 mm, 3µm, Merck) using methanol/water (3/2) as solvent A and isopropanol/methanol (4/1) as solvent B at a flow rate of 0.2 mL/min. All solvents are supplemented with 0.1% HCCOOH and 10 mM ammonium formate. 10 µL of samples were injected and the percentage of solvent B during the gradient elution was the following: 0–20 min, 45%; 40 min, 60%; 50 min, 80%. The column temperature was kept at 40 °C. Mass spectrometry analysis was performed in the positive ionization mode. Mass spectrometry data were treated using the MultiQuant software (ABSciex). Nitrogen was used for the curtain gas (set to 35), gas 1 (set to 40), and gas 2 (set to 40). Needle voltage was at +5500 V with needle heating at 350 °C; the declustering potential was

+10 V. The collision gas was also nitrogen; was set between 26 to 45 eV according to the lipid classes. The dwell time was set to 5 ms. MRM transitions are presented in **Supplemental Table S1**.

Results

The rationale to reveal the lipidome and proteome of Arabidopsis plasma membrane (AtPM) is shown in **Figure 1**. Plasma membrane purified from Arabidopsis suspension cells were spited in two parts: one to identify and quantify the whole PM proteome, the other to identify and quantify the whole PM lipidome on a three-fold method: first, quantification of lipid moieties, then quantification of each lipid class, and finally identification and semi-quantification of all molecular species.

Protein profiling

PM fractions were isolated from Arabidopsis Col-0 cell suspensions by applying the conventional two-phase partition procedure (**37**) to a preparation of total membranes (microsomal fraction). The purity of the three independent AtPM preparations from microsomes (Atμ) was estimated first from enzymatic assays. A major part (85% ± 1, n = 3) of the total ATPase activity associated with the PM fraction was vanadate-sensitive, indicating that PM contamination by tonoplast and other membranes displaying ATPase activities (ER, mitochondria, plastids) was at most 15%. The protein composition of the three crude microsomal fractions and the corresponding PM fractions were further quantitatively analyzed by LC-MS/MS after trypsin digestion of the samples. Using at least two peptides for correct protein assignment and a probability of peptide misidentification inferior to 0.01, a total of 3,948 non-redundant plant proteins were overall identified in the six fractions originating from microsomes (n = 3) and PM (n = 3) preparations (**Supplemental Table S2**). To achieve a posteriori validation of the enrichment in PM proteins and depletion of contaminants with a larger set of protein markers, we implemented a digital immunoblotting workflow according to Zhang and Peck (**43**). To favor experimentally known localization over the use of *in silico* algorithmic predictors for protein localization (**50**), we combined the MS-based quantification of proteins having a unique and experimentally supported subcellular localization. For that purpose, a normalized spectral abundance

factor (NSAF) was calculated for each protein in the six replicates (three biological replicates X two preparations) (**Supplemental Table S2).** Further, an experimentally known subcellular localization was searched for each protein against SUBA5 and Araport11, as inferred from HDA (Inferred from High Throughput Direct Assay) and IDA (Inferred from Direct Assay) GO experimental evidence codes for cellular components (**Supplemental Table S3).**

As summarized in **Supplemental Table S4**, out of the 3,948 proteins identified, 3,745 (94.8%) proteins displayed an experimental code for cellular component, and 595 (15.1%) had an exclusive experimentally-inferred subcellular localization. For the latter proteins, we generated a western-blot *in silico* by adding up all the protein NSAF values recorded for each subcellular compartment in the microsomal and PM fractions. When comparing between these two fractions the total protein abundance ascribed to an exclusive cellular component, **Figure 2** shows that the AtPM preparation was significantly enriched in PM-resident proteins with a reproducible purity of 86% (± 1.4, n = 3), and depleted of proteins assigned to other cellular components with the exception of vacuolar proteins (*p*-value = 0.08). The average abundance of experimentally assigned PM proteins retrieved in the purified PM fraction was 2.2-fold higher than that in the microsomal fraction, an enrichment superior to what previously observed on the basis of SUBA predictions (**43**). Relative to microsomes, the amount of Golgi, mitochondrial and cytosolic proteins was significantly decreased by more than tenfold in the PM fraction (**Figure 2**). Extracellular proteins, recorded as the most abundant contamination, did not exceed 3.1% of the PM fraction in terms of spectral counts (**Figure 2**). Depletion of other contaminants ranged from 2.3 (plastid, cytoskeleton) to 3 (nucleus, endoplasmic reticulum). Overall, digital immunoblotting supports the enrichment in proteins assigned to the PM with a purity estimated to 86%, as inferred from exclusive and experimentally demonstrated protein localization, and in full consistency with the enzymatic characterization.

Characterization of the Arabidopsis PM proteome

Using the criteria described above for protein identification, 2,666, 2,281 and 2,875 proteins were retrieved in the first, second and third AtPM preparation, respectively (**Supplemental Table S4)**.

When retaining only those co-identified in the three replicates, the AtPM proteome of Arabidopsis Col-0 cells was hereby defined as a core-set of 2,165 proteins (**Supplemental Table S5**), which on average cover 98% of total PM spectral abundance (**Supplemental Table S4)**. Among them, a total of 194 proteins were undetected in the three Atμ fractions (e.g. protein kinases, protein phosphatases 2C, oxysterol binding proteins, early nodulin-like protein), which accounted for 2.3% of NSAF, indicating that low abundance proteins have been enriched by the two-phase partition procedure. Many of the 2,165 identifications turned out to be canonical PM markers as determined by alternative methods for localization including fusion proteins with fluorescent reporters. Noteworthy, these PM landmarks included nitrate transporters (AT1G12110, AT4G21680), ammonium transporter 2 (AT2G38290), protein phosphatase 2C (AT3G51370), phospholipase D (AT4G35790), NOD26-like intrinsic protein (AT4G18910), YELLOW STRIPE like 2 protein (AT5G24380), cellulose synthase (AT5G09870), BRI1-like proteins (AT3G13380, AT1G55610), respiratory burst oxidase (AT1G64060), BAK1-interacting receptor-like kinase 1 (AT5G48380) and remorins (AT2G45820, AT3G61260) (**Supplemental Table S5**).

To obtain a functional overview of the Arabidopsis PM proteome, we used Mercator for automated protein function annotation**,** according to the MapMan scheme. Among the 2,165 proteins co-identified in the three PM fractions, 1,818 proteins (84%) were assigned to 32 known functional categories. Two MapMan designations were missing, namely polyamine synthesis (numerical code 22) and micro RNA/natural antisense (numerical code 32), while the undefined/hypothetical function encompassed 347 proteins (**Supplemental Table S5**). To further assess their relative abundance, we added up each of the protein NSAF value recorded within a functional category. **Figure 3A** shows the distribution of spectral counts within the eight MapMan categories displaying a NSAF sum superior to 3%. Signaling (e.g. MAP kinases, 14-3-3 proteins, G-proteins, receptor kinases), protein (e.g. synthesis, folding, modification, destination, degradation) and transport (e.g. ATPases, or transporters of sugars, amino acids, metabolites, ions, metals) were the three prominent functional group with a NSAF of 17, 16 and 15%, respectively. The next top-ranked functions included non-assigned proteins (9.3%), the cell category (8.7%) gathering proteins involved in cell organization, cell cycle, cell

trafficking and vesicular transport, a pool of 8.7%, proteins responsive to stress, a family of miscellaneous enzyme (4.1%, e.g. glycosyl hydrolases, glutathione s-transferases, galactosidases), and proteins related to lipid metabolism (3.4%). When combining lipid metabolism with proteins involved in phosphoinositide signalling and lipid transport according to MapMan, ARALIP and Uniprot annotations, we retrieved a set of 133 lipid-related proteins (**Table S6**). These proteins were classified in different categories according to their substrate and/or their function with 18 proteins associated to phosphoinositides and signaling (e.g. PI4-kinases, PI-PLC, PI phosphatases), 29 to lipid transport and trafficking (e.g. phospholipid-transporting ATPases, lipid transfer proteins), 36 to phospholipid metabolism (e.g. phospholipases, lysophospholipases, DAG kinases), 14 to sterol metabolism (e.g. sterol 3-beta-glucosyltransferase, delta(14)-sterol reductase), 6 to sphingolipid metabolism (e.g. LCB kinases) and 36 to FA metabolism (e.g. acyl-CoA oxidases, long chain acyl-CoA synthetases). Of note, 89 of these proteins were either enriched in PM vs microsomes or only detected only in the AtPM fraction.

In terms of total spectral counts, the top three major abundant proteins encompassed two H^+-ATPases and SKU5, a lipid-anchored protein involved in cell wall expansion (**Supplemental Table S5**). Taken together, these results are consistent with typical functional features of plant PM proteomes reported in previous studies (**30**, **32**, **51**).

Next, we examined the putative mechanisms by which the core-set of 2,165 proteins associate to the PM according to web-based predictor tools (**Supplemental Table S5**), and compared the relative contribution of predicted peripheral and integral membrane proteins to spectral abundance. **Figure 3B** shows that the 736 predicted integral membrane proteins with one or more hydrophobic TM domains spanning the lipid bilayer with an α-helical structure, accounted for 35% of total NSAF, as previously observed in Arabidopsis (**52**). A much higher proportion of NSAF abundance (65%) was assigned to proteins with no predicted TM domains (1,429 proteins). Among the latter, lipid-anchored proteins covalently attached to different FA acyl chains on the cytoplasmic side of the cell membrane via palmitoylation, myristoylation, or prenylation, represented the most abundant category (34% of spectral counts). S-palmitoylation, a post-translational modification mediating the reversible addition

of palmitate and other long-chain fatty acids to proteins at cysteine residues, was predicted as the prominent single lipid modification targeting peripheral proteins to the membrane (NSAF of 16.6%). Predicted secreted proteins with a glycosylphosphatidylinositol (GPI) anchor represent 4% of the total NSAF. Overall, a total of 627 proteins (27% of PM spectral abundance) with no predicted TM domain displayed neither a SP nor a lipid anchor, among which a large majority (79%) was previously identified as PM resident proteins. These results point to alternative mechanisms mediating peripheral membrane association, such as lipid-binding domains (LBDs) that allow protein targeting to membranes by stereospecific interactions with a given phospholipid species (**53**, **54**). In Arabidopsis, 483 LBD-containing proteins have been described (**55**). Within the set of PM proteins lacking a TM domain and a lipid anchor, the identification for example of several C2-containing phospholipases D and Sec14-like proteins, support a role for LBDs in targeting proteins to the PM (**Table S5**).

To compare the hydrophobicity of predicted integral and peripheral membrane proteins, the AtPM proteome was explored in terms of GRAVY score, with positive and negative values referring to hydrophobic and hydrophilic proteins, respectively. **Figure 3C** showed that the 2,165 proteins displayed a GRAVY hydrophobicity between -1.2 and +0.8, as observed in previous plant PM proteome repertoires (**56**, **57**), with 21% of NSAF corresponding to positive GRAVY scores. The results in **Figure 3C** also clearly indicated that predicted integral and peripheral membrane proteins had different hydrophobicity patterns. Namely, the GRAVY index of the peripheral membrane proteins predicted within the PM proteome ranged from -1.2 to +0.2, and only 4% of peripheral protein spectral counts accounted for strictly positive GRAVY values. The same analysis performed on putative integral proteins underlined a GRAVY repartition between -1.2 to and +1, with a significantly larger spectral abundance (54%) of hydrophobic proteins. Consistent with the hydrophobicity of TM segments (**58**), this comparison showed a higher enrichment in hydrophobic proteins within the predicted integral membrane protein fraction of the PM proteome relative to the predicted peripheral fraction. On the basis of a cytoplasmic pH of 7.5 in plant cells (**59**), we examined the distribution of isoelectric points (pIs) retrieved in the AtPM proteome. The results shown in **Figure 3D** indicated that 66.5 and 33.5% of PM spectral counts displayed a pI below and above 7.5,

respectively. In agreement with this result, all proteomes analysed so far usually showed a bimodal pattern resulting in two sets of acidic and basic proteins (**60**). Nonetheless, pI distributions were quite different between predicted integral and non-integral AtPM proteomes with basic proteins accounting for 51.5 and 23.8% of spectral abundance, respectively. Of note, Schwartz et al. (**61**) similarly reported that integral membrane proteomes are enriched in basic proteins due to the basic residues commonly found on membrane spanning helices.

Because TM domain properties of integral membrane proteins act as major determinants of intracellular localization (**62**, **63**, **64**), we further assessed using the TMHMM-2.0 algorithm the quantitative distribution of TM domain-containing proteins in the AtPM proteome. Results indicated that single-spanning (i.e. bitopic) TM proteins ranked first in terms of abundance, accounting for 30% of the spectral counts recorded for all predicted integral membrane proteins (**Figure 4A**). In addition, **Figure 4B** shows that the length of TM α-helical segments of bitopic proteins varied from 15 to 23 amino acids, with an overwhelming majority of 23-residue length, both in terms of protein number (77%) and cumulative protein spectral abundance (84%). Genome-wide bioinformatics analysis agree with this result, as they revealed that in Arabidopsis a large proportion (31%) of predicted bitopic proteins resides in PM, with fewer proteins located in ER, Golgi apparatus, and intracellular organelles (**65**).

Identification of new PM-associated proteins in Arabidopsis

For a comprehensive survey of the number and identity of proteins commonly identified between the current study and other Arabidopsis PM repertoires, an experimentally known residence in the PM of Arabidopsis was searched for each of the 2,165 proteins against SUBA5 and Araport11. According to HDA and IDA evidence codes for cellular components, we retrieved 1,759 (81%) proteins previously recorded as PM proteins, resulting in the reproducible identification of 406 new PM-associated proteins, (**Supplemental Table S7**). The former and the latter fraction accounted for 94.5% and 5.5% of total spectral counts, respectively, indicating that new PM candidates represented a minor quantitative part of AtPM. In addition, the amount of proteins undetected in the three Atμ fractions

was significantly higher (8.9%) within the new PM proteome relative to the other (1.9%), comforting an increased coverage of low abundant proteins in the former fraction. To assess the extent to which web-based tools predict a cellular component localization for the 406 new proteins associated to the PM of Arabidopsis, we further retrieved non-HDA/non-IDA codes searched against Araport11 together with SUBA5 all predictors and SUBA5 consensual prediction. The results listed in **Table S7** showed that 252 (62.1%) proteins accounting for 59.1% of spectral abundance had no predicted localization to the plasma membrane, supporting the existence of cryptic PM proteins.

Both known and new PM fractions were characterized as previously described. With regard to functions (**Figure 5A**), the eight MapMan categories displaying a NSAF sum superior to 3% were similar for both fractions, but new PM-associated proteins showed in terms of spectral counts a significantly higher proportion of candidates assigned to numerical codes 11 (lipid metabolism), 26 (miscellaneous enzyme families) and 35 (not assigned). With special emphasis to lipid-related proteins (**Supplemental Table S6**), the new PM-associated candidates enriched in AtPM relative to microsomes notably included phosphatidylinositol 4-kinase alpha 2 (AT1G51040), two oxysterol binding proteins (AT1G13170, AT4G12460), and phospholipase D beta 2 (AT4G00240).

On the opposite, new PM candidates were significantly depleted of proteins assigned to stress, transport and signaling (**Figure 5A**), including among other features the noticeable absence of heat shock proteins together with the under-representation of leucine-rich repeat protein kinases (5.1%), relative to the corresponding spectral abundance assigned to experimentally known proteins (20.6%). Although the number of proteins without an assigned function may largely limit the functional grouping of data, this observation underlines that both fractions may have different roles when associated to the PM.

When comparing the relative contribution of predicted peripheral and integral membrane proteins to spectral counts within the two fractions, **Figure 5B** indicates that the abundance of TM-containing proteins (integral) was significantly lower within new PM candidates (27.3%) than within the already experimentally-assigned PM proteins (35.3%). In parallel, a much larger proportion of spectral counts was assigned to putative peripheral proteins (no TM domains) in the new PM fraction, including

predicted exoplasmic peripheral proteins, lipidated (prenylated, myristoylated) and non-lipidated cytoplasmic peripheral proteins. Taken together, these results indicate that new PM-associated proteins may be more hydrophilic than previous experimentally known PM proteins. Consistently, 16.7% of spectral counts of the new At PM proteome accounted for strictly positive GRAVY values, while a significantly (p-value = 0.007) higher proportion (21.7%) of hydrophobic proteins was assigned to the experimentally demonstrated PM fraction (**Figure 5C**). Likewise, **Figure 5D** showed that known and new PM proteins also differed (p-value < 10^{-3}) in their pI distribution with a more acidic proteome (74% NSAF) for new PM candidates relative to known PM proteins (66.1% NSAF). This comparison supports a depletion of basic integral proteins in the new PM fraction (**61**).

In agreement with the results of digital immunoblotting (**Figure 2**), new AtPM proteins only consisted of a small set (18.7%) of proteins exclusively localized to the PM when compared to the 330 multi-localizing proteins (MLPs) recorded according to experimental evidence codes (**Supplemental Table S8**). The recurrent identification of these proteins in the three AtPM fractions of this study indicated that these MLPs should not be discarded as contaminants, but rather argued for proteins shuttling or operating across organelles to regulate metabolic reactions or to transmit information from the surrounding environment (**66**). Within this line, the extracellular space and the Golgi apparatus were the two major co-localizing cellular components for the 112 MLPs, each accounting for 74 and 69 proteins, respectively. MapMan grouping further highlighted protein targeting and cell vesicle transport (21 proteins), protein synthesis and degradation (15 proteins), developmental and protein G signalling (11 proteins), and lipid metabolism (10 proteins), as the main functional categories for the 112 MLPs (**Supplemental Table S8**). Taken together, these results support the view that partner location with Arabidopsis PM proteins are involved in developmental processes, transport, signal transduction, cell organization and biogenesis (**67**), with MLPs in the secretory pathway reflecting directional protein trafficking (**68**).

Lipid profiling

Lipidomic analysis have tremendously evolved in the last years. Mass spectrometry methods such as LC-MS/MS are widely used to determine the diversity of the molecular species. The quantification by LC-MS/MS is yet hampered because the ionization yield and the response of the MS analyzer depend on the nature of the lipid and the chemical environment called the matrix. In addition, the molar response varies from one class of lipid to another as between homologs within a class depending on the nature of the fatty acid attached to the glycerol or to the long chain base backbone, and the energy collision (**69**). The need of appropriate standard for all lipids being a limitation, absolute quantifications using LC-MS/MS methods is very difficult. Therefore, following several previous works which tackle lipid quantification (**70**, **71**), we used here a combination of three different analytical methods for lipid identification and quantification (**Figure 1**). First, methanolic hydrolysis of PM lipids and analysis by gas chromatography coupled to mass spectrometry (GC-MS) allowed the quantification of sterols, long-chain fatty acids (FA), and very long-chain fatty acids (VLCFA) using internal dedicated standards. Second, the lipids were separated by high performance thin layer chromatography (HPTLC), scratched, hydrolysed and quantified by GC-MS. Third, the precise identification and regiolocalisation (when possible) of the molecular species of each lipid were determined by liquid chromatography coupled with mass spectrometry (LC-MS/MS) in multiple reaction monitoring (MRM) mode.

Quantification of the three classes of lipids

As described for the protein profiling, we first performed an absolute quantification of total lipids found in the microsomal and PM fractions, together with fresh Arabidopsis suspension cells. After full acid hydrolysis of lipids, corresponding lipid moieties were analyzed and quantified by GC-MS method (see Experimental Procedures). It was assumed that the amount of sterol moieties represents the total sterol content, LCFAs were mostly esterified in glycerolipids and (h)VLCFAs amidified in sphingolipids (**72**). Representative chromatograms are shown in **Supplemental Figure S1**. As expected, palmitic (C16:0) and oleic acid (C18:2) acids were the major LCFAs, even if chains harboring 18 carbon atoms with 0 to 3 double bounds were also detected (**Supplemental Figure S1A,**

B). VLCFA with up to 26 carbon atoms, odd and even number of carbons, 2-hydroxylated or not were also quantified, lignoceric acid (C24:0) and 2-hydroxylated with 24 carbon atoms acid (h24:0) being the major species (**Supplemental Figure S1A)**. Concerning the sterols (free and conjugated) analyzed after shorter acid hydrolysis, mostly β-sitosterol was detected in AtPM, with minor amount of campesterol but no stigmasterol (**Supplemental Figure S1C**).

The molar percentage of each class of lipids was estimated from these amounts of LCFA, (h)VLCFA and sterol moieties using an average molecular molar mass of 750g/mol for glycerolipids, 1200 g/mol for sphingolipids and 400 g/mol for sterols. **Figure 6A** shows that glycerolipids were by far the major lipids of fresh Arabidopsis suspension cells and microsomal fractions with only 10 mol% of sterol and 3 mol% of sphingolipids. These two latter classes were strongly enriched in the AtPM fraction, where glycerolipids, sphingolipids and sterols were distributed equally, with ca. 30 mol% each. Saturated FAs (mostly palmitic, lignoceric and h24:0) were strongly enriched in the AtPM compared to the microsomal fractions (**Figure 6B**), making the PM the most saturated membrane of the plant cell. The VLCFAs identified were mainly not hydroxylated and with FA chains up to C26 (**Figure 6C, D**). From AtPM lipid amount determination, the mass ratio of lipid/protein was calculated to be around 0.8 ± 0.03, in frame of previously described literature (**72**).

Quantification of the major lipids by TLC coupled to GC-MS

After separation by HP-TLC, individual lipid classes were scratched, hydrolyzed and quantified by GC-MS, allowing to determine the amount of AtPM major lipids. Note that minor lipids, barely detectable by TLC, were analyzed by LC-MS/MS (see below). First, HP-TLC allowed the separation of free and conjugated sterols. GC-MS quantification showed that free sterols were the most abundant followed by ASG and SG, with 83.7, 13.5, and 2.6 mol% of total sterols, respectively (**Figure 7A**). Second, glycerolipids and GlcCer were separated by HP-TLC. GC-MS quantification showed that PC and PE were the two major phosphoglycerolipids, representing 47.7 and 24.8 mol% of total glycerolipids, respectively, PI and PS representing 10.5 and 8.3 mol% of total phospholipids, respectively **(Figure 7B**). A few percent of PG were detected in AtPM whereas MGDG and DGDG were barely detectable (less than 0.1 mol%). Finally, GlcCer represents 16.8 mol% of total

sphingolipids (**Figure 7C**). We failed to separate GIPC by HPTLC likely because of the presence of residual PEG-Dextran in the lipid extract perturbates the solvent migration. Therefore we quantified them by LC-MS/MS. As plant GIPC standards are not commercially available, cauliflower GIPC, which are very similar to Arabidopsis GIPCs, were purified and quantified by GC-MS (**Supplemental Figure S3A, B)**. AtPM extracts were injected in LC-MS/MS methods using purified cauliflower GIPC as external standards. This allowed us to fully exploit the LC-MS/MS data and estimate the GIPC amount in AtPM. We determined that Hex(R1)-HexA-IPC and Hex-Hex(R1)-HexA-IPC represent ca. 63.8 and 10.3 mol% of total sphingolipids, respectively (**Figure 7C)**.

Extensive identification and regiolocalisation of lipid molecular species by LC-MS/MS

To obtain a precise determination of molecular species (fatty acid content and position), the different lipid extracts (see Experimental Procedures) were analyzed by LC-MS/MS. We set up MRM methods dedicated to the detection of major glycerolipids (PC, PE, PG, MDGD, DGDG), anionic phospholipids (PA, PS, PI, PIP, PIP_2) and sphingolipids (LCB, LCB-P, Cer, GlcCer and GIPC series: Hex(R1)-HexA-IPC, Hex-Hex(R1)-HexA-IPC). These MRM methods can potentially detect 964 different molecules, see **Supplemental Table S1. Supplemental Figure S2** presents the results obtained for each class of lipids.

For glycerolipids, we showed that PC contain mostly C16 and C18 FA. The major PC species were 34:1, 34:2, 36:1, and 36:3. No VLCFA-containing PC were detected. PE molecules also contain C16 and C18 FA, with few percent of VLCFA up to 24 carbon atoms, with 34:1, 34:2 and 36:3 being the major species. Fragmentation of PE molecules allowed the regiolocalisation of FA found in *sn*-1 and *sn*-2. (Note that this was not possible for PC because it losts the polar head, and not the fatty acid in positive ionization mode). This revealed that major PE molecular species were PE 34.2 (16:0/18:2), PE 34.1 (16:0/18:1), and PE 36.3 (18:2/18:1). Traces of MGDG 34:2, 34:3 and DGDG 34:2, 34:3 were detected but represented less than 0.1% of total glycerolipids (**Figure 7B**, **Supplemental Figure S2**).

Sphingolipids were further analyzed by LC-MS/MS as described in Groux et al. (**73**). We failed to detect LCB- and LCB-phosphate, probably because they were below the limit of detection. The major ceramide species were t18:1/C24:0, t18:1/h24:0 and t18:1/h24:1. The major Hex-Hex(R1)-HexA-IPC were d18:0/h24:0 and d18:0/h24:1 (**Supplemental Figure S2**).

Analysis of anionic phospholipids.

Anionic phospholipids like PA, PS, PI, PIP, and PIP2 were barely detectable by TLC or by LC-MS/MS following the classical method described previously. Thus, a dedicated derivatization step was added to increase the sensitivity of detection (**Figure 1)**, as described in Genva et al. (**49**), Ito et al. (**74**), and Yin et al. (**75**). This derivatization step by methylation using diazomethane remarkably enhanced the ionization, the separation of each peaks and the limit of detection and quantification for each individual anionic phospholipid, more particularly PA, PS, and PIP_2. Applied to AtPM, this sensitive method gave access to the determination of molecular species of anionic lipids.

Relative quantification using internal standards revealed that PI 34.1 and PI 36.1 represent the major PI molecular species (**Figure 8**). The major molecular species of PS contain VLCFA with 42:1, namely fatty acids up to 24 to 26 carbon atoms (**Figure 8**). PS represent 8.3 mol% of total glycerolipids (**Figure 7B**). We also determined that the major molecular species of PA were 34:1 and 36:1, whereas no VLCFA was detected in PA (**Figure 8**). PA represent around 4.3 mol% of total glycerolipids (**Figure 7B**). Concerning the polyphosphoinositides, PIP represent only 1.75 mol % of total phospholipids with 34:1 and 36:1 species. Only traces of PIP_2 were detected with also consisting of 34:1 and 36:1 species (**Figure 7B, 8**).

Full lipidome of AtPM

To summarize, we collected all the lipid profiling data with the major molecular species of each lipid and present them in a single figure, see **Figure 9**. Up to 405 different molecular species in AtPM were detected with GIPC (Hex(R1)-HexA-IPC d18:1/h24:0), PC 36:3, PE 34:2 (16:0/18:2), PS 42:1 and β-sitosterol being the 5 major lipids found in PM purified from *A. thaliana* suspension cells.

Importantly, only traces of MGDG were detected confirming the lack of plastidial contamination, in line with the proteomic data (**Figure 2)**. Similarly, DGDG was also barely detectable showing that suspension cells were not deprived in phosphate (**76**). The weak amount of PA, less than 2 mol% (**Figure 9**), emphasized the lack of lipase activation (mostly phospholipase D) during AtPM purification and lipid extraction, a drawback frequently observed during plant membrane lipid analysis (**77**).

Concerning phosphoinositides, PIP represent 0.6 mol % of total lipids and only traces of PIP_2 were detected (**Figures 7B, 8**). This is sound with previous work estimating PIPs to reach 0.2–1% of total cellular phospholipids, as reviewed in Balla et al. (**78**). Unfortunately, our LC-MS/MS method does not allow to characterize the phosphate isomers of these latter polyphosphoinositides, but previous work using genetically encoded biosensors specific to the polar head of phosphoinositides showed that PI4P is the major isomer found in plant PM (**79**, **80**).

The analysis of FA chain unsaturation of AtPM lipids clearly confirms the results of **Figure 6** with a high proportion of saturated or mono-unsaturated fatty acids present both in glycerolipids and sphingolipids, together with the presence of VLCFA in PS and sphingolipids (see **Supplemental Figure S4)**. PC and PE present a wider range of FA unsaturation than PS and PI.

Discussion

An unprecedented repertoire of PM proteins

In this study, we isolated the PM of Arabidopsis and performed proteomic and lipidomic analyses to propose an integrated view of the qualitative and quantitative composition of proteins and lipids of the plant PM. Numerous proteomic studies have been conducted to decipher the PM protein composition of Arabidopsis (**43**, **51**, **56**, **81**, **82**, **83**, **84**, **85**). However, with 3,948 proteins identified in total (**Supplemental Table S2**), and 2,165 proteins reproducibly identified across three replications (**Supplemental Table S5**), our analysis performed on cell suspensions relative to whole plant system or isolated tissues, has generated by far the most comprehensive qualitative and quantitative view yet for Arabidopsis, including 406 new PM-associated candidates. **Supplemental Table S9** provides a

numerical comparison indicating the improvement in PM protein identifications over time that ranged from 102 (**56**) to 2,165 (current study), with a strong positive correlation (R^2 = 0.98) between proteome coverage and available genomic resources (**Supplemental Figure S5**). Besides this linear relationship indicating that our characterization of AtPM benefited from the complete reannotation of the Arabidopsis reference genome (Araporort11, **44**), the identification of in the current PM fraction of many proteins previously indexed in TAIR10 and SUBA5 but undetected in microsomes, also argued for a better resolution of mass spectrometry analysis. Currently, SUBA5 that provides a central resource for exploring Arabidopsis protein subcellular location using fluorescent protein tagging or mass spectrometry encompasses 5,179 experimentally known PM proteins (**45**). As it is well known that the protein composition of the cell membrane largely depends on the cell type, age, developmental phase, and environmental factors (**32**), further analyses performed on different Arabidopsis tissues and experimental conditions are thus expected to increase the coverage of the PM proteome.

The further *in silico* analyses we performed on the 2,165 PM protein set fitted typical traits of the plant PM, as inferred from functional grouping, membrane-anchoring mechanisms, hydrophobicity pattern, pI distribution, and PM-characteristic features of bitopic proteins in terms of TM domain number and length (**Figures 3-4**, **30**, **52**, **61**, **65**). This was also the case of the new PM fraction (406 proteins) with nonetheless subtle but significant variations, including a higher representation of hydrophilic proteins together with an increased proportion of lipid-related metabolism. With a special interest in this category, several proteins described as ER-resident according to fluorescent protein tagging including phosphatidylserine decarboxylase 3 (PSD3), calcium-dependent lipid-binding protein 1 (CLB1), synaptotagmin-1 (SYT1), and synaptotagmin-5 (SYT5), displayed at least a two-fold enrichment in the AtPM proteome relative to microsomes (**Supplemental Table S6**). Although we cannot rule out the possibility of contamination of the AtPM fraction by other cell compartments, the results of digital immunoblotting did not support the ER as a major source of protein contaminants during PM isolation (**Figure 2**).

Instead, examination of previous Arabidopsis proteome datasets rather argues for their close association to the PM, as inferred from the recurrent MS-based identification of these proteins in previous AtPM pools (**Supplemental Table S6**). Consistent with these observations, the PM is known

to form ER–PM membrane contact sites (MCSs), defined as tight and not fused membrane junctions tethered by specific protein complexes that allow direct communication and the exchange of lipids and cellular signals molecules (Ca^{2+}, reactive oxygen species) between organelles (**86**, **87**). SYT1 and SYT5 together with the Ca^{2+}- and lipid-binding protein CLB1 are notably known to form a complex enriched at ER–PM contact sites (**88**). In support for a dual localisation of PM proteins to the ER, PVA11/VAP27-1, SYT3 (**Table S6**) and several multiple C2 lipid-binding domains and transmembrane region proteins (MCTP), namely AtMCTP3 (AT3G57880.1), AtMCTP4 (AT1G51570.1), AtMCTP6 (AT1G22610.1), AtMCTP15/QKY (AT1G74720.1), and AtMCTP16 (AT5G17980.1) were also present in the AtPM proteome (**Supplemental Table S5**). MCTPs that act as ER-PM tethers specifically at plasmodesmata, are proteins that insert into the ER via their transmembrane region while their C2 domains dock to the PM through interaction with anionic phospholipids (**89**). Taken together, our results confirm that the proteomic approach succeeded in identifying proteins closely associated to the plasma membrane.

An exhaustive analysis yielding a complete picture of the lipid composition of Arabidopsis PM

Lipids represent a large and complex class of small molecules with a huge structural diversity which display hydrophobic and amphipathic chemical properties. The lipid composition of the PM has been studied in many plants like in corn (**90**), in the resurrection plant *Ramonda serbica* following dehydration and rehydration (**91**), in *A. thaliana* with regard to cold acclimation (**34**), sterol biosynthetic mutants (**84**), sphingolipids composition (**92**), in oat and rye in relation to freezing tolerance (**33**), or more recently in the halophyte ice plant *M. crystallinum* (**35**). These works bring important piece of knowledge on the plant PM lipid content and its variation upon stress, but classes of lipids were often missing, like GIPC or phosphoinositides because of lack of sensitivity of the methods (e.g. anionic lipids) or the use of not suitable lipid extraction procedures (e.g. GIPC).

Here, we decided to perform a very complete description of the full lipidome of the plant PM both qualitatively and quantitatively, with the determination of exact molecular species in terms of FA positions for some classes of lipids. Because of the complexity of lipids in terms of number of molecules and the lack of standards, our lipid profiling approach necessitates the use of various

technics. LC-MS/MS is a very powerful method to decipher the molecular species of individual lipids, but the quantification is hampered by the lack of standards necessary to quantify the huge diversity of molecules because the detection is sensitive to the nature of the molecule especially with FAs. For example, among the 47,884 lipids species identified in the Lipid Maps database (https://www.lipidmaps.org), only 100 are commercially available as analytical standards. To obtain quantitative data, we thus added in our approach separation of lipids by TLC coupled to GC-MS as described in Khouri et al. (**71**), see **Figure 1**.

We built MRM tables that potentially allow the detection of almost a thousand different lipids molecular species (**Supplemental Table S1**). This enabled us to detect 405 different molecular species in AtPM, (**Figure 8**, **Supplemental Figure S2**), a number of molecules never reached in the study of the lipidome of the plant PM. Our study confirms previously published study on the full lipidome of the plant PM, but gave a further quantitative informations (**Figure 9**). We thus showed that the three classes of lipids represent each 30 mol% and confirmed that GIPC namely Hex(R1)-HexA-IPC are the major sphingolipids in AtPM. This is in line with the results obtained in PM purified from tobacco leaves and BY-2 suspension cells (**72**). GIPC were long forgotten in lipid analysis as they are not soluble in chloroform/methanol mixture and are hence lost in the interface or the aqueous phase. A suitable lipid extraction procedure (**48**) is need to ensure the full extraction of all classes of plant sphingolipids (In this work, we also measured the presence of more glycosylated Hex-Hex(R1)-HexA-IPC (series B) but 7-times less than series A GIPC. This is in agreement with *A.s thaliana* as a conventional Eudicot plant in which GIPC with two saccharides are dominant (**93**). We have previously shown that both GIPC series are likely involved in the formation for membrane domains together with phytosterols (**27**, **72**). We note the presence of GIPC with di-hydroxylated LCB in suspension cell AtPM (**Supplemental Figure S2**), a result which appears at variance with previously reported GIPC in plant PM which contain mostly tri-hydroxylated LCBs (**72**, **94**). One can ask whether the LCB hydroxylase is down-regulated in suspension cells. We failed to detect LCB-LCB-phosphate, although these simple sphingolipids represent circa 1% of total sphingolipids (**94**). Either they are not present in the PM, or as amphiphilic molecules, they may have been lost during the process of PM purification.

Finally, we developed a new protocol to measure the amount anionic lipids PA, PS, PI and PIP representing 1.6, 3.2, 4.1 and 0.6 mol% of total lipids respectively, and only traces of PIP_2 were detected (see **Figure 9)**. These results are in complete coherence with previously published work measuring the amount of lipids *in planta* using genetically encoded biosensors indicating that PIP are enriched in the PM but not PIP_2 (for review see **95**). LC-MS/MS also indicated that FA esterified in anionic lipids contain 16 or 18 carbon atoms with the notable exception of VLCFA found esterified in PS. These results are similar to what was published previously for the FA content of PA and PI in *A thaliana* (**96**). The DAG moieties of PIP and PIP_2 are the same than the ones detected in PI which indicates that polyphosphoinositides are metabolically derived from PI without any further fatty acyl editing. By contrast to PA, PI and PIPs, we found VLCFA esterified in PS (PS42:1, PS42:2 and to a lesser extend PS40:1 and PS42:3, see **Figure 8**). This is consistent with other previously published studies of PS extracted from Arabidopsis roots or seedlings analyzed by LC-MS/MS (**79**, **96**).

To summarize concerning anionic phospholipids, we provide here an LC-MS/MS method (**49**) that not only confirmed previous published results on the composition of individual classes of anionic phospholipids, but substantially improved their detection and quantification in one-shot. The presence of VLFCA in PS seems a specificity of the plant kingdom. It is interesting to point that PS in animal cells mostly contains 18:0-20:4 fatty acids (**97**). The subcellular localization of PS varies during root cell differentiation and this gradient of localization tunes auxin signaling through the nano-clustering of the small GTPase ROP6 (**98**).

A lipid composition consistent with plant PM as an ordered mosaic of domains

Numerous evidences have pointed to the critical role of lipid acyl chains in membrane organization, in particular through two main properties: (i) the length of acyl chains, (ii) the ratio between saturated and unsaturated bonds along them (**99**), together with the presence of a hydroxylation at the 2 position able to modulate the propensity to interact with sterols and other lipids (**100**). Using the quantitative data related to the 405 lipid molecular species here identified, global characteristics of Arabidopsis PM could be evidenced regarding such properties.

A striking result coming from these analyses is the clear predominance (56%) of fully saturated fatty acyl chains, the second in terms of representativeness being acyl chains harboring one unsaturation (18%) (**Figure 6**). A gradual enrichment of saturated PL species at the expense of monounsaturated species along the secretory pathway (ER > Golgi > PM) has been consistently evidenced in mammalian cells (**101**). This feature can be put in perspective with the increase in membrane order observed along the secretory pathway (**97**). Indeed, experimental data together with molecular dynamics simulation of varying membrane compositions showed that the proportion of saturated acyl chains is positively correlated with the order level of the membrane (**101**, **102**). It has been shown in particular that vesicles formed from a total extract of plant PM lipids exhibit a slightly higher order level than vesicles formed of an equimolar mix of DOPC/DPPC/cholesterol (**28**). The high proportion of saturated FA chains identified in this study is thus in agreement with previous findings suggesting that the plant PM is highly ordered (**27**). The fundamental role of the monounsaturated/saturated ratio for elementary functions (from protective barrier to high trafficking) has been underlined and their biophysical characteristics mainly studied, either in a comparative way or in combination: namely, polyunsaturated PLs notably exhibit specific molecular properties, in particular a high capacity of adaptation towards mechanical stress (**99**, **101**). This agrees with the fact that PM from animal cells appear as “built for stability” whereas ER or Golgi membranes are characterized as highly dynamic, with significantly lower proportion of sterols and sphingolipids (**103**).

It is also interesting to consider the respective contributions of the different lipids to this global feature (see **Supplemental Figure S4**). Indeed, it is clear than sphingolipids (GIPC and GlcCer) are mainly involved in the saturation of PM since more than 70% of their fatty acyl chains exhibit no unsaturation and the remaining 30% only one unsaturation. Regarding phospholipids, PS and PI are the more saturated with 75 and 80%, respectively, of their molecular species with one acyl chain saturated and the other monounsaturated. Conversely, for PC and PE molecular species with one acyl chain saturated and the other monounsaturated are a minority (about 30% each), whereas molecules with two or more (up to 6) unsaturations are prevalent. Results presented here might thus point to a differential involvement of plant lipids in the various aspects of PM functioning, the “barrier function” being mainly ensured by sphingolipids (which also play a role in perception of environmental changes

and subsequent signaling), whereas PC and PE might be mostly involved in the global adaptive processes. The presence of mainly monounsaturated PS is also consistent with the visualization of stable PS nanodomains on Arabidopsis root tip cell PM (**98**).

Another parameter to consider is the high diversity of molecular species present on the membrane, belonging to the different classes previously identified as major actors of membrane organization. Indeed, it has been extensively described that the combination of lipids harboring specific properties due to their chemical structures is a key regulator of membrane organization, from the nano to the microscale (**104**).

A noticeable information from the data presented here is the presence on the PM of 30 mol% of sterols mainly sitosterol and campesterol which are the two free phytosterols with the highest ordering properties (**28**, **105**). Moreover, conjugated sterols (SG and ASG) which were also demonstrated as very efficient to increase membrane order, in combination with free sterols (**28**), have also been identified in significant proportion (13% and 3% of the total sterol amount, respectively). This also contributes, together with saturation, to build the vision of a rather ordered plant PM. Moreover, sterols have been demonstrated to be not only key determinants of the plant PM global order *in vivo*, but also involved in the presence of ordered domains within this membrane (**20**, **26**, **27**, **28**). Sitosterol and campesterol have been proven particularly efficient in this respect, and the relative proportion of phospholipids (saturated and unsaturated), GIPC and sterols (free and conjugate) identified in this study is quite similar to the one providing a high level of ordered domain formation in the membrane of lipid unilamellar vesicles (**28**). This high amount of sterols, sphingolipids and saturated FA is thus fully supporting the presence within plant PM of ordered domains, in line with the « lipid raft » hypothesis that proposed rafts as PM nanodomains of high molecular order, enriched in cholesterol and sphingolipids, in which proteins involved in signaling can selectively interact with effector molecules (**106**). The fact that the VLCFAs of the sphingolipids (either GIPC or GlcCer) are mostly saturated is quite consistent with such a view of the plant PM.

A finely tuned adjustment of the molecular characteristics of lipids and proteins

Global analysis of the molecular characteristics of PM proteins identified reveals interesting features. In particular, it indicates than more than 80% of bitopic proteins (which represent by far the most abundant category of TM proteins identified) exhibit a transmembrane helix comprising 23 amino acids (**Figure 4**). These data support a model wherein long TM domains (≥ 23 amino acids) direct plasma membrane localization (**107**). This was further confirmed by Brandizzi et al. (**108**) who demonstrated that in plants among the different TM domains tested (from 17 to 23 aa), only TM segments with 23 aa drove proteins to the PM, while shorter TM domains (17 and 20 residues) remain mostly in ER and Golgi compartments, respectively.

The need to adjust the length of protein TM helices and the thickness of the hydrophobic core of the lipid bilayer to prevent or minimize a mismatch leading to a distortion of the bilayer or the protein, was identified for a long time as a crucial parameter (**9**). This suggested that the length of acyl chains, determining the thickness of the bilayer might be well suited to the length of protein domains spanning the membrane. This was very nicely demonstrated, comparing two species of the yeast *Schizosaccharomyces* with lipids exhibiting significant differences regarding the length of their FA chains: experiments coupled with bioinformatic analysis revealed that the length of protein TM domains were higher in the strain with the longest FA chains, and that reducing the carbon number of these FA chains resulted in a mistargeting of proteins (**29**). In the present study, lipidomic data indicate that about 30% of the lipids (phospholipids and sphingolipids) have one FA chains with at least 20 carbons. Thus, it seems that the characteristics of lipid FA chains and TM domains of bitopic proteins, quite specific to the PM, are very well adjusted one to another.

The plasma membrane is enriched in proteins involved in lipid metabolism, signaling and transport

The PM constitutes the outer border of the cell, therefore implying a crucial role in mediating communication between the cell interior and its surrounding environment. As a result, this study and others (for review see **31**, **32**), overall highlighted a PM proteome composition functionally dominated both in terms of abundance and number by proteins involved in signaling (**Figures 3A**). Nonetheless,

the mining of AtPM proteomic data to emphasize lipid-related proteins according to ARALIP and Uniprot annotations led to the identification of 133 proteins listed in **supplemental Table S5**. This should be considered as a significant amount since it represents more than 6% of the PM proteins identified. Among these 133 proteins, 89 were enriched in PM vs microsomes or detected only in the PM fraction. These proteins are either associated to phosphoinositides and signaling, involved in lipid transport and trafficking, or lipid metabolism.

Of note, except SAC1, all proteins associated to phosphoinositides and signaling are enriched in the PM fraction compared to microsomes, 3 of them (PI4 kinases alpha2 and 2, PI-PLC) being detected only in the PM fraction. This is fully consistent with the recent findings indicating that PI4P, which mainly accumulates at the PM in plant cells (as in this study where it is much more abundant than PIP2), seems to support in plants many functions that are typically attributed to PIP2 in animal and yeast cells and should be considered a hallmark lipid of PM (**109**). Consistently, PI4-kinases alpha 1 and 2, which are enzymes involved in PI4P synthesis, are enriched in AtPM. These enzymes are tethered to the PM by a complex composed of proteins from the NO-POLLEN-GERMINATION EFR3-OF-PLANTS and HYCCIN-CONTAINING families (**110**), which here belong to the AtPM proteome (i.e.: AT5G64090, AT2G41830, AT5G64090, respectively). Enzyme related to PIPs turn-over such as SAC9 and patellins (**111**, **112**) are also found in AtPM (**Table S6**).

Two isoforms of DAG kinases (DGK3 and DAGK7) were enriched in the PM fraction: these enzymes are involved in the production of PA in synergy with PI-PLC, an enzyme detected only in the PM in our analysis (**Table S6**). PI-PLC hydrolyses PIP2 to generate DAG, further phosphorylated by DGK to produce PA. The PA can also be generated through the hydrolysis of structural lipids (such as PC) by PLD: numerous isoforms of PLD are found enriched in the PM fraction (**Table S6**). The presence of this set of enzymes on the PM is thus in agreement with the very low amount of PIP_2 and, conversely, the presence of a significant proportion of PA, which is a central lipid to mediate signaling processes in plants (**113**). The fatty acyl chains associated to PA (36:1 and 34:1) are also the most abundant in PIP2 as in structural lipids such as PC, in agreement with the involvement of these two pathways.

Related to sterol metabolism, it is interesting to point the enrichment on PM and high abundancy of a sterol 3-beta-glucosyltransferase (UGT80A2, see **Supplemental Table S6**). This enzyme catalyzes the synthesis of steryl glycosides (SGs) and acyl steryl glycosides (ASGs). This is in full agreement with the identification of significant amounts of such conjugated sterols on the PM (respectively 13.5 and 2.6% of the total sterols, see **Figure 7**), and consistent with the fact that such enzymes can act on sitosterol, and campesterol, which are the free sterols identified in this study.

Because PM does not participate in autonomous biogenesis of its structural lipids, they must be trafficked to their PM destination or the extracellular space in the case of the cuticle (**114**). This implies a constant flux of lipids from the synthesis compartments, mainly the ER, towards the PM, as mediated by vesicular and non-vesicular routes (**115**). Here, proteins having role in lipid trafficking were enriched for their large majority (93%) in AtPM relative to microsomes, including SYTs, VAPs, ORPs, and phosphatidylinositol transfer proteins (PIPT) of the SEC14-like family (**Supplemental Table S6**). SYT proteins are composed of a lipid transfer domain involved in lipid traffic between the ER and the PM (**116**). Lack of SYT1 and SYT3 increases the accumulation of DAG during cold stress, indicating an important role of SYTs in lipid metabolism and PM integrity (**117**). Of note, PI4P is critical for the localization of tethering proteins to the PM, including SYT1 (**117**) and MTCPs (**89**). VAP proteins interact with several lipid transfer proteins (LTPs), especially from the oxysterol-binding protein (ORP) family at membrane contact sites (**118**, **119**). Several ORPs transport their lipid ligand from the ER in exchange for PI4P on apposed membranes (**120**). PIPTs, which regulate a signalling interface between lipid metabolism and protein transport from the Golgi to the cell surface (**121**), include PM resident AtSFHs and AtPATLs, potentially involved in the regulation of the level and localization of phosphoinositides (**111**). Overall, these results point to the phosphoinositide lipid composition of the PM as a key determinant of membrane trafficking (**79**). Some lipids may also be synthesized by chemical modifications of others and a heavy turnover of lipids also influences the ratio of lipid types in the PM (**27**). For example, numerous phospholipases A2, C and D and phosphodiesterase GDPD were found in the AtPM proteome showing either a remodeling or signaling processes involving lipid polar heads and fatty acids (**122**). In addition, energy-dependent

translocators allow lipids to translocate between the two leaflets of the PM bilayer. Here, two phospholipid-transporting ATPases, ALA1 and ALA3, which may contribute to the asymmetric lipid arrangement of the PM (**123**), were enriched in AtPM relative to microsomes (**Supplemental Table S6**).

Conclusion

This work provides the most complete repertoire to date of the lipids and proteins that make up plant cell PM. The functional and structural characteristics of the identified molecular species support elements already obtained by targeted studies and provide new insights into their ability to interact to shape the identity of this membrane.

This study clearly paves the way towards a crucial and still very poorly known characteristics: the asymmetry of composition and organization of the two leaflets of plant PM. Asymmetry has been thoroughly determined recently in erythrocytes but only few papers tackle this question in plants (**124**, **125**). Importantly, the description of the exact lipidome and the asymmetry is a pre-requirement to embark in the molecular dynamic modelisation of the plant PM, as it was reported in animal PM (**126**), and recently described in plant PM (**127**).

Data availability

The mass spectrometry proteomic data have been deposited to the ProteomeXchange Consortium via the PRIDE (https://www.ebi.ac.uk/pride/) partner repository with the dataset identifier PXD040971. The mass spectrometry lipidomic data have been deposited in the public repository Zenodo (https://zenodo.org) under doi.org/10.5281/zenodo.7925332.

Supplemental data

This article contains supplemental data including figures.

Acknowledgments

The authors wish to thank Jérôme Fromentin for his expertise and support in the generation and maintenance of cell cultures. We thank Bordeaux-Metabolome platform for lipid analysis (https://www.biomemb.cnrs.fr/en/lipidomic-plateform/) supported by Bordeaux Metabolome Facility-MetaboHUB (grant no. ANR–11–INBS–0010 to LF, SM). Proteomics analyses were performed on the PAPPSO platform (http://pappso.inrae.fr) which is supported by INRAE (http://www.inrae.fr), the Ile-de-France regional council (https://www.iledefrance.fr/education-recherche), IBiSA (https://www.ibisa.net) and CNRS (http://www.cnrs.fr). This study received financial support from the French government in the framework of the IdEX Bordeaux University "Investments for the Future" program / GPR Bordeaux Plant Sciences » to LF, SM. This work was supported by the French National Research Agency (grant no. ANR-19-CE20-0016-02 to DB, LF, SM, FSP, PVD). The authors declare that none of the funding sources was involved in study design, collection, analysis and interpretation of data, writing of the manuscript and decision to submit the work for publication.

References

References

1 Singer, S.J., and Nicolson, G.L. (1972) The fluid mosaic model of the structure of cell membranes. *Science*. **175**, 720-31. doi: 10.1126/science.175.4023.720.

2 Nicolson, G.L. (2014) The fluid-mosaic model of membrane structure: still relevant to understanding the structure, function and dynamics of biological membranes after more than 40 years. *Biochim Biophys Acta*. **1838**, 1451-66. doi: 10.1016/j.bbamem.2013.10.019.

3 Jost, P.C., Griffith, O.H., Capaldi, R.A., and Vanderkooi G. (1973) Evidence for boundary lipid in membranes. *Proc Natl Acad Sci U S A*. **70**, 480-4. doi: 10.1073/pnas.70.2.480.

4 Lee, A.G. (2003) Lipid-protein interactions in biological membranes: a structural perspective. *Biochim Biophys Acta*. **1612**, 1-40. doi: 10.1016/s0005-2736(03)00056-7.

5 Duncan, A.L., Song, W., and Sansom, M.S.P. (2020) Lipid-dependent regulation of ion channels and G protein-coupled receptors: Insights from structures and simulations. *Annu Rev Pharmacol Toxicol*. **60**, 31-50. doi: 10.1146/annurev-pharmtox-010919-023411.

6 Hansen, S.B., Tao, X., and MacKinnon, R. (2011) Structural basis of PIP2 activation of the classical inward rectifier K+ channel Kir2.2. *Nature*, **477**, 495-8. doi: 10.1038/nature10370.

7 Katan, M., and Cockcroft, S. (2020) Phosphatidylinositol(4,5)bisphosphate: diverse functions at the plasma membrane. *Essays Biochem*. **64**, 513-531. doi: 10.1042/EBC20200041.

8 Rao, B.D., Shrivastava, S., and Chattopadhyay, A. (2017). Hydrophobic Mismatch in Membranes: When the Tail Matters. In: Chattopadhyay, A. (eds) *Membrane Organization and Dynamics* . Springer Series in Biophysics, vol 20. Springer, Cham. doi: 10.1007/978-3-319-66601-3_16.

9 Jensen, M.Ø., and Mouritsen, O.G. (2004) Lipids do influence protein function-the hydrophobic matching hypothesis revisited. *Biochim Biophys Acta*. **1666**, 205-26. doi: 10.1016/j.bbamem.2004.06.009.

10 Grau, B., Javanainen, M., García-Murria, M.J., Kulig, W., Vattulainen, I., Mingarro, I., and Martínez-Gil, L. (2017) The role of hydrophobic matching on transmembrane helix packing in cells. *Cell Stress*. **1**, 90-106. doi: 10.15698/cst2017.11.111.

11 Espinosa, G., López-Montero, I., Monroy, F., and Langevin, D. (2011) Shear rheology of lipid monolayers and insights on membrane fluidity. *Proc Nat Acad Sci U S A.* **108**, 6008-13. doi: 10.1073/pnas.1018572108.

12 Scarlata, S.F. (1996) The Effects of increased viscosity on the function of integral membrane proteins, in J.L. Markley, D.B. Northrop, and C.A. Royer (eds), *High Pressure Effects in Molecular Biophysics and Enzymology*. Oxford Academic, New York. doi: 10.1093/oso/9780195097221.003.0024.

13 Budin, I., de Rond, T., Chen, Y., Chan, L.J.G., Petzold, C.J., and Keasling, J.D. (2018) Viscous control of cellular respiration by membrane lipid composition. *Science*. **362**, 1186-1189. doi: 10.1126/science.aat7925.

14 Jouhet, J. (2013) Importance of the hexagonal lipid phase in biological membrane organization. *Front Plant Sci*. **4**, 494. doi: 10.3389/fpls.2013.00494.

15 Brohawn, S.G., Su, Z., and MacKinnon, R. (2014) Mechanosensitivity is mediated directly by the lipid membrane in TRAAK and TREK1 K+ channels. *Proc Natl Acad Sci U S A*. **111**, 3614-9. doi: 10.1073/pnas.1320768111.

16 Simons, K., and Ikonen, E. (1997) Functional rafts in cell membranes. *Nature*. **387**, 569-72. doi: 10.1038/42408.

17 Sezgin, E., Levental, I., Mayor S., and Eggeling, C. (2017) The mystery of membrane organization: composition, regulation and roles of lipid rafts. *Nat Rev Mol Cell Biol*. **18**, 361-374. doi: 10.1038/nrm.2017.16.

18 Garcia-Parajo, M.F., Cambi, A., Torreno-Pina, J.A., Thompson, N., and Jacobson, K. (2014) Nanoclustering as a dominant feature of plasma membrane organization. *J Cell Sci*. **127**, 4995-5005. doi: 10.1242/jcs.146340.

19 Bücherl, C.A., Jarsch, I.K., Schudoma, C., Segonzac, C., Mbengue, M., Robatzek, S., MacLean, D., Ott, T., and Zipfel, C. (2017) Plant immune and growth receptors share common signalling components but localise to distinct plasma membrane nanodomains. *Elife*. **6**, e25114. doi: 10.7554/eLife.25114.

20 Gronnier, J., Gerbeau-Pissot, P., Germain, V., Mongrand, S., and Simon-Plas, F. (2018) Divide and rule: Plant plasma membrane organization. *Trends Plant Sci*. **23**, 899-917. doi: 10.1016/j.tplants.2018.07.007.

21 Sandor, R., Der, C., Grosjean, K., Anca, I., Noirot, E., Leborgne-Castel, N., Lochman, J., Simon-Plas, F., and Gerbeau-Pissot, P. (2016) Plasma membrane order and fluidity are diversely triggered by elicitors of plant defence. *J Exp Bot*. **67**, 5173-85. doi: 10.1093/jxb/erw284.

22 Jaillais, Y., and Ott, T. (2020) The Nanoscale organization of the plasma membrane and its importance in signaling: A proteolipid perspective. *Plant Physiol*. **182**, 1682-1696. doi: 10.1104/pp.19.01349.

23 Veatch, S.L., and Keller, S.L. (2005) Seeing spots: complex phase behavior in simple membranes. *Biochim Biophys Acta*. **1746**, 172-85. doi: 10.1016/j.bbamcr.2005.06.010.

24 Baumgart, T., Hammond, A.T., Sengupta, P., Hess, S.T., Holowka, D.A., Baird, B.A., and Webb, W.W. (2007) Large-scale fluid/fluid phase separation of proteins and lipids in giant plasma membrane vesicles. *Proc Natl Acad Sci U S A*. **104**, 3165-70. doi: 10.1073/pnas.0611357104.

25 Eggeling, C., Ringemann, C., Medda, R,. Schwarzmann, G,. Sandhoff, K., Polyakova, S., Belov, V.N., Hein, B., von Middendorff, C., Schönle, A., and Hell, S.W. (2009) Direct

observation of the nanoscale dynamics of membrane lipids in a living cell. *Nature*. **457**, 1159-62. doi: 10.1038/nature07596.

26 Gerbeau-Pissot, P., Der, C., Thomas, D., Anca, I.A., Grosjean, K., Roche, Y., Perrier-Cornet, J.M., Mongrand, S., and Simon-Plas F. (2014) Modification of plasma membrane organization in tobacco cells elicited by cryptogein. *Plant Physiol*. **164**, 73-86. doi: 10.1104/pp.113.225755.

27 Mamode Cassim, A., Gouguet, P., Gronnier, J., Laurent, N., Germain, V., Grison, M., Boutté, Y., Gerbeau-Pissot, P., Simon-Plas, F., and Mongrand, S. (2019) Plant lipids: Key players of plasma membrane organization and function. *Prog Lipid Res*. **73**:1-27. doi: 10.1016/j.plipres.2018.11.002.

28 Grosjean, K., Mongrand, S., Beney, L., Simon-Plas, F., and Gerbeau-Pissot, P. (2015) Differential effect of plant lipids on membrane organization: specificities of phytosphingolipids and phytosterols. *J Biol Chem* **290**, 5810-25. doi: 10.1074/jbc.M114.598805.

29 Makarova, M., Peter, M., Balogh, G., Glatz, A., MacRae, J.I., Lopez Mora, N., Booth, P., Makeyev, E., Vigh, L., and Oliferenko, S. (2020) Delineating the rules for structural adaptation of membrane-associated proteins to evolutionary changes in membrane lipidome. *Curr Biol*. **30**, 367-380.e8. doi: 10.1016/j.cub.2019.11.043.

30 Yadeta, K.A., Elmore, J.M., and Coaker, G. (2013) Advancements in the analysis of the Arabidopsis plasma membrane proteome. *Front Plant Sci*. **4**, 86. doi: 10.3389/fpls.2013.00086

31 Komatsu, S., and Hashiguchi, A. (2018) Subcellular proteomics: Application to elucidation of flooding-response mechanisms in soybean. *Proteomes*.**6**, 13. doi: 10.3390/proteomes6010013.

32 Shishova, M.F., and Yemelyanov, V.V. (2021) Proteome and lipidome of plant cell membranes during development. *Russ J Plant Physiol*. **68**, 800–17. doi: 10.1134/S1021443721050162.

33 Uemura, M., and Steponkus, P.L. (1994) A Contrast of the plasma membrane lipid composition of oat and rye leaves in relation to freezing tolerance. *Plant Physiol*. **104**, 479-496. doi: 10.1104/pp.104.2.479.

34 Uemura, M., Joseph, R.A., and Steponkus, P.L. (1995) Cold acclimation of *Arabidopsis thaliana* (Effect on plasma membrane lipid composition and freeze-induced lesions). *Plant Physiol*. **109**, 15-30. doi: 10.1104/pp.109.1.15.

35 Guo, Q, Liu, L, Rupasinghe, TWT, Roessner, U, and Barkla, BJ. (2022) Salt stress alters membrane lipid content and lipid biosynthesis pathways in the plasma membrane and tonoplast. *Plant Physiol*. **189**, 805-826. doi: 10.1093/plphys/kiac123.

36 Stanislas, T., Bouyssie, D., Rossignol, M., Vesa, S., Fromentin, J., Morel, J., Pichereaux, C., Monsarrat, B., and Simon-Plas, F. (2009) Quantitative proteomics reveals a dynamic association of proteins to detergent-resistant membranes upon elicitor signaling in tobacco. *Mol Cell Proteomics*. **8**, 186-98. doi: 10.1074/mcp.

37 Larsson, C., Sommarin, M., and Widell, S. (1994) Isolation of highly purified plant plasma membranes and separation of inside-out and right-side-out vesicles. *Meth Enzymol.* **228**, 451-469.

38 Briskin, D.P., Leonard, R.T., and Hodges, T.K. (1987). Isolation of the plasma membrane: Membrane markers and general principles. *Meth Enzymol.* **148**, 542-558.

39 Craig, R., and Beavis, R.C. (2004) TANDEM: matching proteins with tandem mass spectra. *Bioinformatics*. **20**, 1466-1467. doi: 10.1093/bioinformatics/bth092.

40 Langella, O., Valot, B., Balliau, T., Blein-Nicolas, M., Bonhomme, L., and Zivy, M. (2017) X!TandemPipeline: A tool to manage sequence redundancy for protein inference and phosphosite identification. *J Proteome Res*. **16**, 494-503. doi: 10.1021/acs.jproteome.6b00632.

41 Zybailov, B., Mosley, A.L., Sardiu, M.E., Coleman, M.K., Florens, L, and Washburn, M.P. (2006) Statistical analysis of membrane proteome expression changes in *Saccharomyces cerevisiae*. *J Proteome Res.* **5**, 2339-2347. doi: 10.1021/pr060161n.

42 Staehr, P., Löttgert, T., Christmann, A., Krueger, S., Rosar, C., Rolčík, J., Novák, O., Strnad, M., Bell, K., Weber, A.P., Flügge, U.I., and Häusler, R.E., 2014. Reticulate leaves and stunted

roots are independent phenotypes pointing at opposite roles of the phosphoenolpyruvate/phosphate translocator defective in cue1 in the plastids of both organs. *Front Plant Sci*. 5, 126. 10.3389/fpls.2014.00126.

43 Zhang, Z.J., and Peck, S.C. (2011) Simplified enrichment of plasma membrane proteins for proteomic analyses *in Arabidopsis thaliana*. *Proteomics*. **11**, 1780-1788. doi: 10.1002/pmic.201000648.

44 Cheng, C.Y., Krishnakumar, V., Chan, A.P., Thibaud-Nissen, F., Schobel, S., and Town, C.D. (2017) Araport11: a complete reannotation of the *Arabidopsis thaliana* reference genome. *Plant J*. **89**,789-804.

45 [dataset] Hooper, C.M., Castleden, I., Tanz, S.K., Grasso, S.V., Aryamanesh, N., and Millar, A.H. (2022) Subcellular localisation database for Arabidopsis proteins version 5. doi:10.26182/8dht-4017.

46 Lohse, M., Nagel, A., Herter, T., May, P., Schroda, M., Zrenner, R., Tohge, T., Fernie, A.R., Stitt, M., and Usadel, B. (2014) Mercator: a fast and simple web server for genome scale functional annotation of plant sequence data. *Plant Cell Environ*. **37**, 1250-1258. doi: 10.1111/pce.12231.

47 Li-Beisson, Y., Shorrosh, B., Beisson, F., Andersson, M.X., Arondel, V., Bates, P.D., Baud, S., Bird, D., Debono, A., Durrett, T.P., Franke, R.B., Graham, I.A., Katayama, K., Kelly, A.A., Larson, T., Markham, J.E., Miquel, M., Molina, I., Nishida, I., Rowland, O., Samuels, L., Schmid, K.M., Wada, H., Welti, R., Xu, C., Zallot, R., and Ohlrogge, J. (2013) Acyl-lipid metabolism. *Arabidopsis Book*. **11**, e0161. doi: 10.1199/tab.0161.

48 Toledo, M.S., Suzuki, E., Straus, A.H., and Takahashi, H.K. (1995) Glycolipids from *Paracoccidioides brasiliensis.* Isolation of a galactofuranose-containing glycolipid reactive with sera of patients with paracoccidioidomycosis. *J Med Vet Mycol*. **33**, 247-51. doi: 10.1080/02681219580000501.

49 [preprint] Genva, M., Fougere L., Bahammou, D., Mongrand, S., Boutte, Y., Fouillen, and Fouillen, L. (2023) A global LC-MS^2-based methodology to identify and quantify anionic phospholipids in plant samples. bioRxiv. doi: 10.1101/2023.05.10.539967.

50 Nair, R., and Rost, B. (2002) Sequence conserved for subcellular localization. *Protein Sci*. **11**, 2836-2847. doi: 10.1110/ps.0207402.

51 Miki, Y., Takahashi, D., Kawamura, Y., and Uemura, M. (2019) Temporal proteomics of Arabidopsis plasma membrane during cold- and de-acclimation. *J Proteomics*. **15**, 71-81. doi: 10.1016/j.jprot.2018.11.008.

52 Marmagne, A., Ferro, M., Meinnel, T., Bruley, C., Kuhn, L., Garin, J., Barbier-Brygoo, H., and Ephritikhine, G. (2007) A high content in lipid-modified peripheral proteins and integral receptor kinases features in the arabidopsis plasma membrane proteome. *Mol Cell Proteomics.* **6**, 1980-96. doi: 10.1074/mcp.M700099-MCP200.

53 Petit, J.D., Immel, F., Lins, L., and Bayer, E.M. (2019) Lipids or proteins: Who is leading the dance at membrane contact sites? *Front Plant Sci*. **10**, 198. doi: 10.3389/fpls.2019.00198.

54 Noack, L.C., and Jaillais, Y. (2020) Functions of anionic lipids in plants. *Annu Rev Plant Biol.* **29**, 71-102. doi: 10.1146/annurev-arplant-081519-035910.

55 de Jong, F., and Munnik, T. (2021) Attracted to membranes: lipid-binding domains in plants. *Plant Physiol*. **185**, 707-723. doi: 10.1093/plphys/kiaa100.

56 Marmagne, A., Rouet, M.A., Ferro, M., Rolland, N., Alcon, C., Joyard, J., Garin, J., Barbier-Brygoo, H., and Ephritikhine, G. (2004) Identification of new intrinsic proteins in Arabidopsis plasma membrane proteome. *Mol Cell Proteomics*. **3**, 675-691. doi: 10.1074/mcp.M400001-MCP200.

57 Morel, J., Claverol, S., Mongrand, S., Furt, F., Fromentin, J., Bessoule, J.J., Blein, J.P., and Simon-Plas, F. (2006) Proteomics of plant detergent-resistant membranes. *Mol Cell Proteomic*s. **5**, 1396-1411. doi: 10.1074/mcp.M600044-MCP200.

58 Whitelegge, J.P. (2013) Integral membrane proteins and bilayer proteomics. *Anal Chem*. **85**, 2558-2568. doi: 10.1021/ac303064a

59 Martinière, A., Gibrat, R., Sentenac, H., Dumont, X., Gaillard, I., and Paris, N. (2018) Uncovering pH at both sides of the root plasma membrane interface using noninvasive imaging. *Proc Nat. Acad Sci U S A.* **115**, 6488-6493. doi: 10.1073/pnas.1721769115.

60 Kiraga, J., Mackiewicz, P., Mackiewicz, D., Kowalczuk, M., Biecek, P., Polak, N., Smolarczyk, K., Dudek, M.R., and Cebrat, S. (2007) The relationships between the isoelectric point and: length of proteins, taxonomy and ecology of organisms. *BMC Genomics*. **12**, 8:163. doi: 10.1186/1471-2164-8-163.

61 Schwartz, R., Ting, C.S., and King, J. (2001) Whole proteome pI values correlate with subcellular localizations of proteins for organisms within the three domains of life. *Genome Res.* **11**, 703-709. doi: 10.1101/gr.gr-1587r.

62 Cosson P., Perrin J., and Bonifacino, J.S. (2013) Anchors aweigh: protein localization and transport mediated by transmembrane domains. *Trends Cell Biol*. **23**, 511-7. doi: 10.1016/j.tcb.2013.05.005.

63 Sharpe, H.J., Stevens, T.J., and Munro, S. (2010) A comprehensive comparison of transmembrane domains reveals organelle-specific properties. *Cell*. **9**, 158-169. doi: 10.1016/j.cell.2010.05.037.

64 Singh, S., and Mittal, A. (2016) Transmembrane domain lengths serve as signatures of organismal complexity and viral transport mechanisms. *Sci Rep*. **6**, 22352. doi: 10.1038/srep22352.

65 Pogozheva, I.D., and Lomize, A.L. (2018) Evolution and adaptation of single-pass transmembrane proteins. *Biochim Biophys Acta Biomembr*. **1860**, 364-377. doi: 10.1016/j.bbamem.2017.11.002.

66 Xiong, E., Cao, D., Qu, C., Zhao, P., Wu, Z., Yin, D., Zhao, Q., and Gong F. (2022) Multilocation proteins in organelle communication: Based on protein-protein interactions. *Plant Direct*. **6**, e386. doi: 10.1002/pld3.386.

67 Li, S., Ehrhardt, D.W., and Rhee, S.Y. (2006) Systematic analysis of Arabidopsis organelles and a protein localization database for facilitating fluorescent tagging of full-length Arabidopsis proteins. *Plant Physiol*. **141**, 527-39. doi: 10.1104/pp.106.078881.

68 Thul, P.J., and Lindskog, C. (2018) The human protein atlas: A spatial map of the human proteome. *Protein Science*. **27**, 233-244. doi: 10.1002/pro.3307.

69 Pulfer, M., and Murphy, R.C (2003) Electrospray mass spectrometry of phospholipids. *Mass Spectrom Rev*. **22**, 332–364. doi: 10.1002/mas.10061.

70 Jouhet, J., Lupette, J., Clerc, O., Magneschi, L., Bedhomme, M., Collin, S., Roy, S., Maréchal, E., and Rébeillé, F. (2017) LC-MS/MS versus TLC plus GC methods: Consistency of glycerolipid and fatty acid profiles in microalgae and higher plant cells and effect of a nitrogen starvation. *PLoS One*. **12**, e0182423. doi: 10.1371/journal.pone.0182423.

71 Khoury, S., Canlet, C., Lacroix, M.Z., Berdeaux, O., Jouhet, J., and Bertrand-Michel, J. (2018) Quantification of lipids: Model, reality, and compromise. *Biomolecules*. **8**, 174. doi: 10.3390/biom8040174.

72 Cacas, J.L., Buré, C., Grosjean, K., Gerbeau-Pissot, P., Lherminier, J., Rombouts, Y., Maes, E., Bossard, C., Gronnier, J., Furt, F., Fouillen, L., Germain, V., Bayer, E., Cluzet, S., Robert, F., Schmitter, J.M., Deleu, M., Lins, L., Simon-Plas, F., and Mongrand, S. (2016) Revisiting plant plasma membrane lipids in tobacco: A focus on sphingolipids. *Plant Physiol*. **170**, 367-84. doi: 10.1104/pp.15.00564.

73 Groux, R., Fouillen, L., Mongrand, S., and Reymond, P. (2022) Sphingolipids are involved in insect egg-induced cell death in Arabidopsis. *Plant Physiol*. **189**, 2535-2553. doi: 10.1093/plphys/kiac242.

74 Ito, Y., Esnay, N., Platre, MP, Wattelet-Boyer, V, Noack, LC, Fougère, L, Menzel, W, Claverol, S, Fouillen, L, Moreau, P, Jaillais, Y, and Boutté, Y.(2021) Sphingolipids mediate polar sorting of PIN2 through phosphoinositide consumption at the trans-Golgi network. *Nat Commun*. **12**, 4267. doi: 10.1038/s41467-021-24548-0.

75 Yin, Y., Raboanatahiry, N., Chen, K., Chen, X., Tian, T., Jia, J., He, H., He, J., Guo, Z., Yu, L., and Li, M. (2022) Class A lysophosphatidic acid acyltransferase 2 from Camelina sativa promotes very long-chain fatty acids accumulation in phospholipid and triacylglycerol. *Plant J*. **112**, 1141-1158. doi: 10.1111/tpj.15999.

76 Jouhet, J., Maréchal, E., Baldan, B., Bligny, R., Joyard, J., and Block, M.A. (2004) Phosphate deprivation induces transfer of DGDG galactolipid from chloroplast to mitochondria. *J Cell Biol*. **167**, 863-74. doi: 10.1083/jcb.200407022.

77 Shiva, S., Enninfu, R., Roth, .M.R., Tamura, P., Jagadish, K., and Welti, R. (2018) An efficient modified method for plant leaf lipid extraction results in improved recovery of phosphatidic acid. *Plant Methods*. **14**, 14. doi: 10.1186/s13007-018-0282-y.

78 Balla, T. (2013) Phosphoinositides: tiny lipids with giant impact on cell regulation. *Physiol Rev*. **93**, 1019-137. doi: 10.1152/physrev.00028.2012.

79 Platre, M.P., Noack, L.C., Doumane, M., Bayle, V., Simon, M.L.A., Maneta-Peyret, L., Fouillen, L., Stanislas, T., Armengot, L., Pejchar, P., Caillaud, M.C., Potocký, M., Čopič, A., Moreau, P., and Jaillais, Y. (2018) A Combinatorial lipid code shapes the electrostatic landscape of plant endomembranes. *Dev Cell*. **45**, 465-480.e11. doi: 10.1016/j.devcel.2018.04.011.

80 Furt, F., Simon-Plas, F., and Mongrand, S. (2011). Lipids of the plant plasma membrane, in: Murphy, A., Schulz, B., Peer, W. (eds) *The Plant Plasma Membrane*. Plant Cell Monographs, vol 19. Springer, Berlin, Heidelberg. doi: 10.1007/978-3-642-13431-9_1.

81 Alexandersson, E., Saalbach, G., Larsson, C., and Kjellbom, P. (2004) Arabidopsis plasma membrane proteomics identifies components of transport, signal transduction and membrane trafficking. *Plant Cell Physiol*. **45**, 1543-56. doi: 10.1093/pcp/pch209.

82 Nelson, C.J., Hegeman, A.D., Harms, A.C., and Sussman, M.R. (2006) A quantitative analysis of Arabidopsis plasma membrane using trypsin-catalyzed (18)O labeling. *Mol Cell Proteomics.* **5**, 1382-95. doi: 10.1074/mcp.M500414-MCP200.

83 Elmore, J.M., Liu, J., Smith, B., Phinney, B., and Coaker, G. (2012) Quantitative proteomics reveals dynamic changes in the plasma membrane during Arabidopsis immune signaling. *Mol Cell Proteomics*. **4**, M111.014555. doi: 10.1074/mcp.M111.014555.

84 Zauber H., Burgos, A., Garapati, P., and Schulze, W.X. (2014) Plasma membrane lipid-protein interactions affect signaling processes in sterol-biosynthesis mutants in *Arabidopsis thaliana*. *Front Plant Sci*. **5**, 78. doi: 10.3389/fpls.2014.00078.

85 de Michele, R., McFarlane, H.E., Parsons, H.T., Meents, M.J., Lao, J., González Fernández-Niño, S.M., Petzold, C.J., Frommer, W.B., Samuels, A.L., and Heazlewood, JL. (2016) Free-flow electrophoresis of plasma membrane vesicles enriched by two-phase partitioning enhances the quality of the proteome from Arabidopsis seedlings. *J Proteome Res*. **15**, 900-13. doi: 10.1021/acs.jproteome.5b00876.

86 Bayer, E.M., Sparkes, I., Vanneste, S., and Rosado, A. (2017) From shaping organelles to signalling platforms: the emerging functions of plant ER-PM contact sites. *Curr Opi. Plant Biol*. **40**, 89-96. doi: 10.1016/j.pbi.2017.08.006.

87 Baillie, A.L., Falz, A.L., Müller-Schüssele, S.J., and Sparkes, I. (2020) It started with a kiss: Monitoring organelle interactions and identifying membrane contact site components in plants. *Front Plant Sci*. **11**, 517. doi: 10.3389/fpls.2020.00517.

88 Lee, E., Santana, B.V.N., Samuels, E., Benitez-Fuente, F., Corsi, E., Botella, M.A., Perez-Sancho, J., Vanneste, S., Friml, J., Macho, A., Azevedo, A.A., and Rosado, A. (2020) Rare earth elements induce cytoskeleton-dependent and PI4P-associated rearrangement of SYT1/SYT5 endoplasmic reticulum-plasma membrane contact site complexes in Arabidopsis. *J Exp Bot*. **71**, 3986-3998. doi: 10.1093/jxb/eraa138.

89 Brault, M.L., Petit, J.D., Immel, F., Nicolas, W.J., Glavier, M., Brocard, L., Gaston, A., Fouché, M., Hawkins, T.J., Crowet, J.M., Grison, M.S., Germain, V., Rocher, M., Kraner, M., Alva, V., Claverol, S., Paterlini, A., Helariutta, Y., Deleu, M., Lins, L., Tilsner, J., and Bayer, E.M. (2019) Multiple C2 domains and transmembrane region proteins (MCTPs) tether membranes at plasmodesmata. *EMBO Rep*. **20**, e47182. doi: 10.15252/embr.201847182.

90 Bohn, M., Heinz, E., and Lüthje, S. (2001) Lipid composition and fluidity of plasma membranes isolated from corn (*Zea mays* L.) roots. *Arch Biochem Biophys*. **387**, 35-40. doi: 10.1006/abbi.2000.2224.

91 Quartacci, MF, Glisić, O, Stevanović, B, and Navari-Izzo, F. (2002) Plasma membrane lipids in the resurrection plant *Ramonda serbica* following dehydration and rehydration. *J Exp Bot*. **53**, 2159-66. doi: 10.1093/jxb/erf076.

92 Carmona-Salazar, L., Cahoon, R.E., Gasca-Pineda, J., González-Solís, A., Vera-Estrella, R., Treviño, V., Cahoon, E.B., and Gavilanes-Ruiz, M. (2021) Plasma and vacuolar membrane sphingolipidomes: composition and insights on the role of main molecular species. *Plant Physiol*. **186**, 624-639. doi: 10.1093/plphys/kiab064.

93 Cacas, J.L., Buré, C., Furt, F., Maalouf, J.P., Badoc, A., Cluzet, S., Schmitter, J.M., Antajan, E., and Mongrand, S. (2013) Biochemical survey of the polar head of plant

glycosylinositolphosphoceramides unravels broad diversity. *Phytochemistry*. **96**, 191-200. doi: 10.1016/j.phytochem.2013.08.002.

94 Markham, J.E., Li., J, Cahoon, E.B., and Jaworski, J.G. (2006) Separation and identification of major plant sphingolipid classes from leaves. *J Biol Chem*. **281**, 22684-94. doi: 10.1074/jbc.M604050200.

95 Platre, M.P., and Jaillais, Y. (2017) Anionic lipids and the maintenance of membrane electrostatics in eukaryotes. *Plant Signal Behav*. **12**, e1282022. doi: 10.1080/15592324.2017.1282022.

96 Devaiah, S.P., Roth, M.R., Baughman, E., Li, M., Tamura, P., Jeannotte, R., Welti, R., and Wang, X. (2006) Quantitative profiling of polar glycerolipid species from organs of wild-type Arabidopsis and a phospholipase Dalpha1 knockout mutant. *Phytochem* **67**, 1907-24. doi: 10.1016/j.phytochem.

97 Lorent, J.H., Levental, K.R., Ganesan, L., Rivera-Longsworth, G., Sezgin, E., Doktorova, M., Lyman, E., and Levental I. (2020) Plasma membranes are asymmetric in lipid unsaturation, packing and protein shape. *Nat Chem Biol*. **16**, 644-652. doi: 10.1038/s41589-020-0529-6.

98 Platre, M.P., Bayle, V., Armengot, L., Bareille, J., Marquès-Bueno, M.D.M., Creff, A., Maneta-Peyret, L., Fiche, J.B., Nollmann, M., Miège, C., Moreau, P., Martinière, A., and Jaillais, Y. (2019) Developmental control of plant Rho GTPase nano-organization by the lipid phosphatidylserine. *Science*. **364**, 57-62. doi: 10.1126/science.aav9959.

99 Vanni, S., Riccardi, L., Palermo, G., and De Vivo, M. (2019) Structure and dynamics of the acyl chains in the membrane trafficking and enzymatic processing of lipids. *Acc Chem Res*. 52, 3087-3096. doi: 10.1021/acs.accounts.9b00134.

100 Marquês, J.T., Marinho, H.S., and de Almeida, R.F.M. (2018) Sphingolipid hydroxylation in mammals, yeast and plants - An integrated view. *Prog Lipid Res*. **71**, 18-42. doi: 10.1016/j.plipres.2018.05.001.

101 Antonny, B., Vanni, S., Shindou, H., and Ferreira, T. (2015) From zero to six double bonds: phospholipid unsaturation and organelle function. *Trends Cell Biol*. **25**, 427-36. doi: 10.1016/j.tcb.2015.03.004.

102 Borges-Araújo, L., Domingues, M.M., Fedorov, A., Santos, N.C., Melo, M.N., and Fernandes, F. (2021) Acyl-chain saturation regulates the order of phosphatidylinositol 4,5-bisphosphate nanodomains. *Commun Chem*.**4**, 164. doi: 10.1038/s42004-021-00603-1.

103 van Meer, G., Voelker, D.R., and Feigenson, G.W. (2008) Membrane lipids: where they are and how they behave. *Nat Rev Mo. Cell Biol*. **9**, 112-24. doi: 10.1038/nrm2330.

104 Harayama, T., and Riezman, H. (2018) Understanding the diversity of membrane lipid composition. *Nat Rev Mol Cell Biol*. **19**, 281-296. doi: 10.1038/nrm.2017.138.

105 Beck, J.G., Mathieu, D., Loudet, C., Buchoux, S., and Dufourc, E.J. (2007) Plant sterols in "rafts": a better way to regulate membrane thermal shocks. *FASEB J*. **21**, 1714-23. doi: 10.1096/fj.06-7809com.

106 Simons, K., and Ikonen, E. (1997) Functional rafts in cell membranes. *Nature*. **387**, 569-72. doi: 10.1038/42408.

107 Watson, R.T., and Pessin, J.E. (2001) Transmembrane domain length determines intracellular membrane compartment localization of syntaxins 3, 4, and 5. *Am J Physiol Cell Physiol*. **281**, C215-23. doi: 10.1152/ajpcell.2001.

108 Brandizzi, F., Frangne, N., Marc-Martin, S., Hawes, C, Neuhaus, J.M., and Paris, N. (2002) The destination for single-pass membrane proteins is influenced markedly by the length of the hydrophobic domain. *Plant Cell*. **14**, 1077-92. doi: 10.1105/tpc.000620.

109 Marković, V., and Jaillais, Y. (2022) Phosphatidylinositol 4-phosphate: a key determinant of plasma membrane identity and function in plants. *New Phytol*. **235**, 867-874. doi: 10.1111/nph.18258.

110 Noack, L.C., Bayle, V., Armengot, L., Rozier, F., Mamode Cassim, A., Stevens, F.D., Caillaud, M.C., Munnik, T., Mongrand, S., Pleskot, R., and Jaillais Y.A. (2022) Nanodomain-anchored scaffolding complex is required for the function and localization of phosphatidylinositol 4-kinase alpha in plants. *Plant Cell*. **34**, 302-332. doi: 10.1093/plcell/koab135.

111 Tejos, R., Rodriguez-Furlán, C., Adamowski, M., Sauer, M., Norambuena, L., and Friml, J. (2018) PATELLINS are regulators of auxin-mediated PIN1 relocation and plant development in *Arabidopsis thaliana*. *J Cell Sci*. **131**, jcs204198. doi: 10.1242/jcs.204198.

112 Mao, Y, and Tan, S. (2021) Functions and mechanisms of SAC phosphoinositide phosphatases in plants. *Front Plant Sci*. **12**, 803635. doi: 10.3389/fpls.2021.803635.

113 Pokotylo, I., Kravets, V., Martinec, J., and Ruelland E. (2018) The phosphatidic acid paradox: Too many actions for one molecule class? Lessons from plants. *Prog Lipid Res.* **71**, 43-53. doi: 10.1016/j.plipres.2018.05.003.

114 Hurlock, A.K., Roston, R.L., Wang, K., and Benning C. (2014) Lipid trafficking in plant cells. *Traffic*. **15**, 915-32. doi: 10.1111/tra.12187.

115 Michaud, M., and Jouhet, J. (2019) Lipid trafficking at membrane contact sites during plant development and stress response. *Front Plant Sci*. **15**, 10:2. doi: 10.3389/fpls.2019.00002.

116 Qian, T., Li, C., Liu, F., Xu, K., Wan, C., Liu, Y., and Yu, H. (2022) Arabidopsis synaptotagmin 1 mediates lipid transport in a lipid composition-dependent manner. *Traffic*. **23**, 346-356. doi: 10.1111/tra.12844.

117 Ruiz-Lopez, N., Pérez-Sancho, J., Del Valle, A.E., Haslam, R.P., Vanneste, S., Catalá, R., Perea-Resa, C., Damme, D.V., García-Hernández, S., Albert, A., Vallarino, J., Lin, J., Friml, J., Macho, A.P., Salinas, J., Rosado, A., Napier, J.A., Amorim-Silva, V., and Botella, M.A. (2021) Synaptotagmins at the endoplasmic reticulum-plasma membrane contact sites maintain diacylglycerol homeostasis during abiotic stress. *Plant Cell*. **33**, 2431-2453. doi: 10.1093/plcell/koab122.

118 Murphy, S.E., and Levine, T.P. (2016) VAP, a versatile access point for the endoplasmic reticulum: Review and analysis of FFAT-like motifs in the VAPome. *Biochim Biophys Acta*. **1861**, 952-961. doi: 10.1016/j.bbalip.2016.02.009.

119 Saheki, Y, De Camilli, P. (2017) Endoplasmic reticulum-plasma membrane contact sites. *Annu Rev Biochem*. **86**, 659-684. doi: 10.1146/annurev-biochem-061516-044932.

120 Nakatsu, F., and Kawasaki, A. (2021) Functions of oxysterol-binding proteins at membrane contact sites and their control by phosphoinositide metabolism. *Front Cell Dev Bio*l. **9**, 664788. doi: 10.3389/fcell.2021.664788.

121 Bankaitis, V.A., Aitken, J.R., Cleves, A.E., and Dowhan, W. (1990) An essential role for a phospholipid transfer protein in yeast Golgi function. *Nature*. **347**, 561-2. doi: 10.1038/347561a0.

122 Wang, L, Shen, W, Kazachkov, M, Chen, G, Chen, Q, Carlsson, AS, Stymne, S, Weselake, RJ, and Zou, J. (2012) Metabolic interactions between the Lands cycle and the Kennedy pathway of glycerolipid synthesis in Arabidopsis developing seeds. *Plant Cell*. **24**, 4652-69. doi: 10.1105/tpc.112.104604.

123 López-Marqués R.L. (2023) Mini-review: Lipid flippases as putative targets for biotechnological crop improvement. *Front Plant Sci*. **14**, 1107142. doi: 10.3389/fpls.2023.1107142.

124 Takeda, Y., and Kasamo, K. (2001) Transmembrane topography of plasma membrane constituents in mung bean (*Vigna radiata* L.) hypocotyl cells. I. Transmembrane distribution of phospholipids. *Biochim Biophys Acta*. **1513**, 38-48. doi: 10.1016/s0005-2736(01)00342-x.

125 Tjellström, H., Hellgren, L.I., Wieslander, A., and Sandelius, A.S. (2010) Lipid asymmetry in plant plasma membranes: phosphate deficiency-induced phospholipid replacement is restricted to the cytosolic leaflet. *FASEB J*. **24**, 1128-38. doi: 10.1096/fj.09-139410.

126 Ingólfsson, H.I., Melo, M.N., van Eerden, F.J., Arnarez, C., Lopez, C.A., Wassenaar, T.A., Periole, X., de Vries, A.H., Tieleman, D.P., and Marrink, S.J.(2014) Lipid organization of the plasma membrane. *J Am Chem Soc*. **136**, 14554-9. doi: 10.1021/ja507832e.

127 Klauda, JB. (2018) Perspective: Computational modeling of accurate cellular membranes with molecular resolution. *J Chem Phys*. **149**, 220901. doi: 10.1063/1.5055007.

128 Mamode Cassim, A., Navon, Y., Gao, Y., Decossas, M., Fouillen, L., Grélard, A., Nagano, M., Lambert, O., Bahammou, D., Van Delft, P., Maneta-Peyret, L., Simon-Plas, F., Heux, L., Jean, B., Fragneto, G., Mortimer, J.C., Deleu, M., Lins, L., and Mongrand, S. (2021) Biophysical analysis of the plant-specific GIPC sphingolipids reveals multiple modes of membrane regulation. *J Biol Chem*. **296**, 100602. doi: 10.1016/j.jbc.2021.100602.

Figures legends

Figure 1. Rationale for the determination of AtPM proteome and AtPM lipidome. Plasma membrane purified form *Arabidopsis thaliana* suspension cells were splited in two parts: one to identify and quantify the whole proteome, the other to identify and quantify the whole lipidome on three-fold methods. First, quantification of lipid moieties after hydrolysis and quantification by Gas Chromatography coupled to mass spectrometry (GC-MS) using internal standards. Second, quantification of each lipid class after separation by High-Performance-Thin Layer Chromatography (HP-TLC), scratched of the lipids, hydrolysis and further quantification by GC-MS) using internal standards. Third, identification and semi-quantification of all molecular species by Liquid-Chromatography coupled to MS using internal standards.

Figure 2. Comparative subcellular distribution of the proteins experimentally localized to an exclusive cellular component according to GO inference between microsomal (Atμ) and purified plasma membrane (AtPM) fractions. Histograms display the average cumulative sum (n = 3) of NSAF values (×100) for each cellular component. Bars represent the standard error of the mean. Asterisks refer to subcellular compartments displaying an abundance significantly (p-value < 0.05) different between the two fractions, as inferred from Welch-test analyses performed after angular transformation of cumulative NSAF data. Nota bene: the extracellular compartment includes cell wall proteins in SUBA5.

Figure 3. Characterization of the core-set of the AtPM proteome of Arabidopsis Col-0 cells. **A**, Distribution into protein functional categories according to MapMan analysis. Only categories accounting for more than 3% of the total PM proteome abundance are presented. **B**, Putative membrane targeting mechanisms according to TMHMM-2.0, SignalP 5.0, NetGPI-1.1, and GPS-Lipid online predictor tools, with TM, SP, Palm, Myr, Prenyl, and GPI refering to TM alpha-helix, N-

terminal signal sequence, S-palmitoylation, N-myristoylation, prenylation, and glypiation, respectively. Comparative distribution of **C**, GRAVY hydrophobicity and **D**, pI values between non-integral proteins (white colour), integral (black colour) and total (grey colour) proteins. Histograms display the average cumulative sum (n = 3) of NSAF values (×100) within each category. Bars represent the standard error of the mean.

Figure 4. Properties of the 736 integral membrane proteins predicted in the AtPM proteome according to TMHMM-2.0. Distribution of **A**, single- and multi-spanning TM proteins, and **B**, TM segment lengths of bitopic proteins. Histograms display the average cumulative sum (n = 3) of NSAF values (×100) within each category. Bars represent the standard error of the mean.

Figure 5. **Comparative features between putative new candidate AtPM proteins (black colour) and previous experimentally known PM proteins (white colour). A,** Distribution into protein functional categories according to MapMan analysis. Only categories accounting for more than 3% of the total abundance are presented. **B**, Putative membrane targeting mechanisms according to TMHMM-2.0, SignalP 5.0, NetGPI-1.1, and GPS-Lipid online predictor tools, with TM, SP, Palm, Myr, Prenyl, and GPI refering toTM alpha-helix, N-terminal signal sequence, S-palmitoylation, N-myristoylation, prenylation, and glypiation, respectively. Comparative distribution of **C**, GRAVY hydrophobicity and **D**, pI values between known and new PM proteins. Histograms display the average cumulative sum (n = 3) of NSAF values (×100) within each category. Bars represent the standard error of the mean. Asterisks refer to categories displaying an abundance significantly (*p*-value < 0.05) different between the two fractions, as inferred from Welch-test analyses performed after angular transformation of cumulative NSAF data.

Figure 6. Quantification of the three lipid classes in fresh Arabidopsis suspension cell, microsomal fraction Atμ, and purified plasma membrane AtPM. A, Quantification by GC-MS of

three major lipid classes namely sterols (green colour), glycerophospholipids (blue colour), and sphingolipids (orange colour) after acidic hydrolysis and derivatization. Experiments were done on fresh Arabidopsis suspension cells, microsomal (Atμ), and PM (AtPM) preparations. Results are shown as the molar percentage (mean ± standard deviation, n = 3). **B**, Unsaturation, **C**, Amount of non- and 2-hydroxylated fatty acids and **D**, number of carbon atom were calculated for the lipid quantified in fresh Arabidopsis suspension cells, Atμ and AtPM.

Figure 7. Lipidome of the Arabidopsis plasma membrane. A, Quantification by HPTLC coupled to GC-MS of sterol classes (FS, free sterol; SG, steryl glycoside; ASG, Acyl steryl glycoside). **B**, Quantification by HPTLC coupled to GC-MS of major glycerolipid classes (PC, PE, PI). Anionic lipids (PA, PS, PI, PIP, PIP_2) were quantified by LC-MS/MS (see Figure 8), and quantification were integrated in the pie chart. **C**, Quantification by HPTLC coupled to GC-MS of GlcCer. Ceramides (Cer) and GIPC (Hex(R1)-HexA-IPC and Hex-Hex(R1)-HexA-IPC) were quantified by LC-MS/MS (see Figure 8), and quantification were integrated in the pie chart. Results are shown as the molar percentage (mean ± standard deviation, n = 3).

Figure 8. LC-MS/MS profiling of minor anionic lipid classes found in AtPM. AtPM anionic lipids namely PI, PS, PA, PIP, PIP_2 were submitted to methylation by diazomethane and injected to LC-MS/MS. Results show the different molecular species expressed as molar percentage (mean ± standard deviation, n = 3).

Figure 9. Lipidome of the Arabidopsis plasma membrane. Lipidomic results were gathered in a single figure showing the amount, expressed as mol%, of the 17 classes of lipids found in the AtPM, and the major molecular species (in square) found in each class of lipids. Abbreviations are as follow: FS, free sterol; SG, steryl glycoside; ASG, PC; phosphatidylcholine, PE; phosphatidylethanolamine, PG; phosphatidylglycerol, PA; phosphatidic acid, PS; phosphatidylserine, PI; phosphatidylinositol,

PIP; phosphatidylinositol monophosphate, PIP_2; phosphatidylinositol bisphosphate, DGDG; digalactosyldiacylglycerol, MGDG; monogalactosyldiacylglycerol, Glysosyl inositol phosphoryl ceramide GIPC series A: Hex(R1)-HexA-IPC and series B Hex-Hex(R1)-HexA-IPC; GlcCer; glucosylceramide, Cer; ceramide.

Supplemental information

SUPPLEMENTAL FIGURES

Figure S1. Quantification of (h)(VLC)FAMES and sterol moieties released after acidic hydrolysis of AtPM preparation. A, Representative GC-MS chromatography showing the separation of (h)VLCFAMES moieties from sphingolipid part. Quantification of the different fatty acids (h)(VLC)FAMES detected by GC-MS. h14 and C17 are the internal standard. **B,** Representative GC-MS chromatography showing the separation of unsaturated FAMES with 0-3 double bonds. Quantification of the different fatty acids FAMES detected by GC-MS. C17 is the internal standard. **C,** Representative GC-MS chromatography of sterol moieties. Quantification of the different sterol moieties with cholestanol as internal standards. Cholestanol is the internal standard. Experiments were done 3 times on independent AtPM preparations, mean (± standard deviation) is shown.

Figure S2. Molecular species analyzed by LC-MS/MS by MRM method of major lipid classes found in AtPM. AtPM preparations were extracted with the different procedure dedicated to the classes of lipids and injected to LC-MS/MS. Results show the different molecular species of PC, PE, PG, DGDG, MGDG, LCB, LCB-P, CerR, GlcCer, Glysosyl inositol phosphoryl ceramide GIPC series A, Hex(R1)-HexA-IPC and series B Hex-Hex(R1)-HexA-IPC. Analyses were performed 3-4 on independent AtPM preparations. cn:d, with n representing the total number of carbons and d the number of unsaturations, the two fatty acids are represented in parenthesis. A dash (-) between the two fatty acids within the nomenclature means that the regiolocation is not known. Conversely, the use of a slash (/) shows that the regiolocalisation is experimentally established.

Figure S3. Purification of cauliflower GIPC series A (Hex(R1)-HexA-IPC) to be used as external standards for LC-MS/MS. GIPC were purified from cauliflower according to (**128)**. **A**, Purified GIPC series A (Hex(R1)-HexA-IPC) were analyzed by TLC and **B**, recisely quantification by GC-MS after acidic hydrolysis and derivatization. **C**, Purified GIPC were injected to LC-MS/MS spiked with GlcCer d18:1/c12:0. By estimating that the response of the purified GIPC in LC-MS/MS is similar to

that of the GIPC contained in the AtPM samples and using the same internal standard GlcCer d18:1/c12:0, we were able to estimate the amount of GIPC present in the AtPM sample.

Figure S4. Unsaturation and chain length of fatty acids for major lipids identified in AtPM.

Figure S5. Relationship between the number of proteins identified in the PM proteome of *A. thaliana* and the number of available protein entries for *A. thaliana*.

SUPPLEMENTAL TABLES

Table S1. MRM tables used in the lipidomic analysis.

Table S2. List of the 3,948 proteins and their corresponding NSAF values obtained from the six fractions analyzed in the current study by using an *E*-value smaller than 10^{-5} as a criterion to assign correct protein identification. Accessions and annotations refer to https://www.araport.org/downloads/Araport11_Release_201606. Corresponding peptide sequences are displayed in sheet 2. µ and PM refer to the microsomal and plasma membrane fractions obtained from three distinct biological experiments, respectively.

Table S3. Experimentally know localization of the 3,948 proteins identified in the current study, as inferred from HDA (Inferred from High Throughput Direct Assay) and IDA (Inferred from Direct Assay) GO experimental evidence codes for cellular components searched againt SUBA5 and Araport11. Accessions and annotations refer to https://www.araport.org/downloads/Araport11_Release_201606. µ and PM refer to the microsomal and plasma membrane fractions obtained from three distinct biological experiments, respectively.

Table S4. Quantitative distribution of the proteins identified in the three microsomal (Atμ) and plasma membrane (AtPM) fractions.

Table S5. *In silico* characterization of the 2,165 proteins corresponding to the core-set of the plasma membrane (PM) proteome of Arabidopsis Col-0 cells when retaining only the proteins co-identified in the three distinct PM replicates analyzed in the current study.

Table S6. List of the 133 lipid-related proteins identified in the AtPM proteome.

Table S7. *In silico* characterization of the 1,759 proteins inferred as experimentally-known PM resident according to HDA (Inferred from High Throughput Direct Assay) and IDA (Inferred from Direct Assay) GO experimental evidence codes for cellular components searched against SUBA5 and Araport11.

Table S8. *In silico* characterization of the 406 proteins inferred as experimentally-unknown PM resident according to HDA (Inferred from High Throughput Direct Assay) and IDA (Inferred from Direct Assay) GO experimental evidence codes for cellular components searched against SUBA5 and Araport11.

Table S9. Comparison of the number of proteins identified over time in the PM proteome of *Arabidopsis thaliana.*

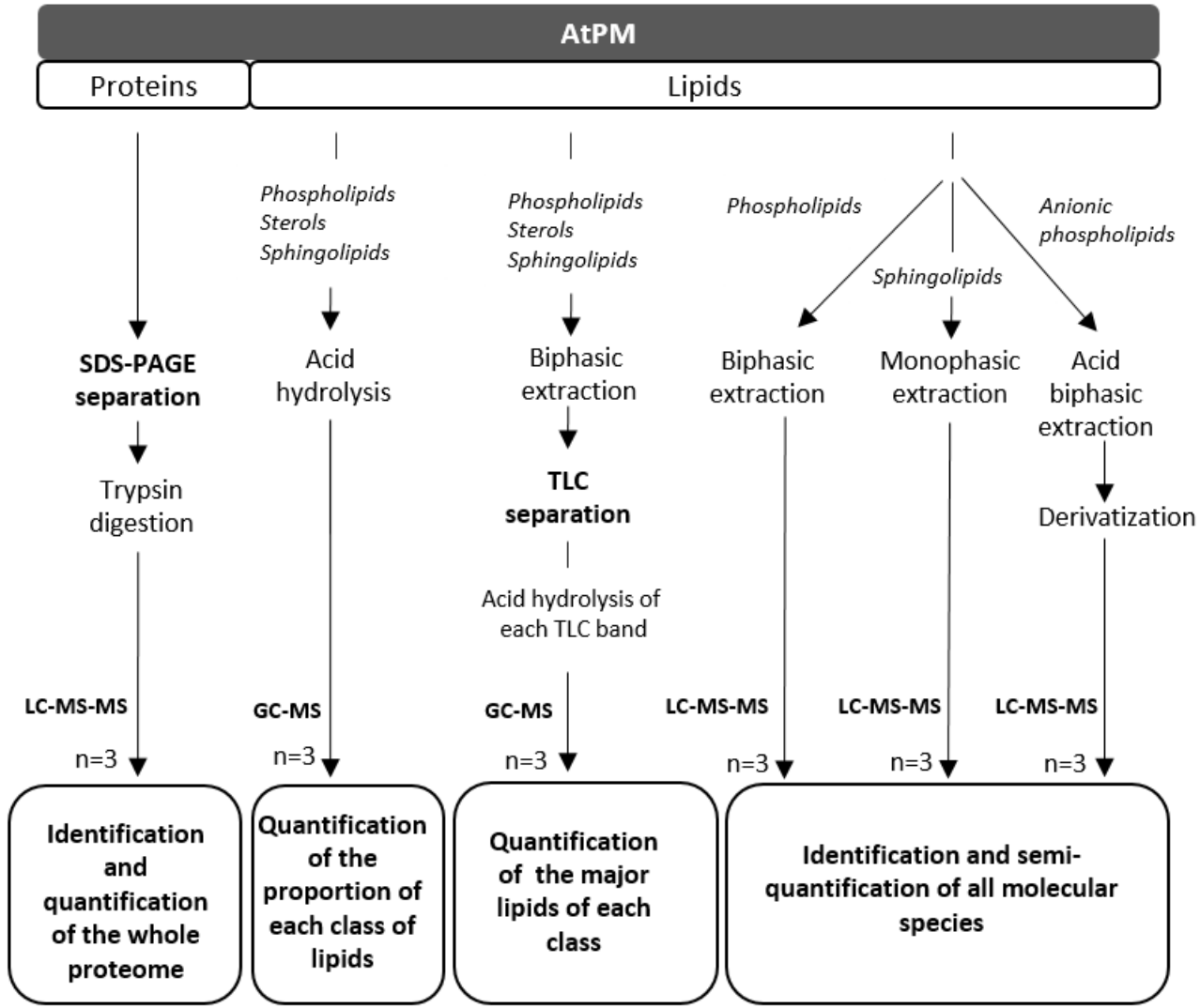
AtPM
Proteins
Lipids
Phospholipids
Sterols
Sphingolipids
Phospholipids
Sterols
Sphingolipids
Phospholipids
Sphingolipids
Anionic
phospholipids
SDS-PAGE
separation
Trypsin
digestion
Acid
hydrolysis
Biphasic
extraction
TLC
separation
Acid hydrolysis of
each TLC band
Biphasic
extraction
Monophasic
extraction
Acid
biphasic
extraction
Derivatization
LC-MS-MS
n=3
GC-MS
n=3
GC-MS
n=3
LC-MS-MS
n=3
LC-MS-MS
n=3
LC-MS-MS
n=3
Identification
and
quantification
of the whole
proteome
Quantification
of the
proportion of
each class of
lipids
Quantification
of the major
lipids of each
class
Identification and semi-
quantification of all molecular
species

Figure 1

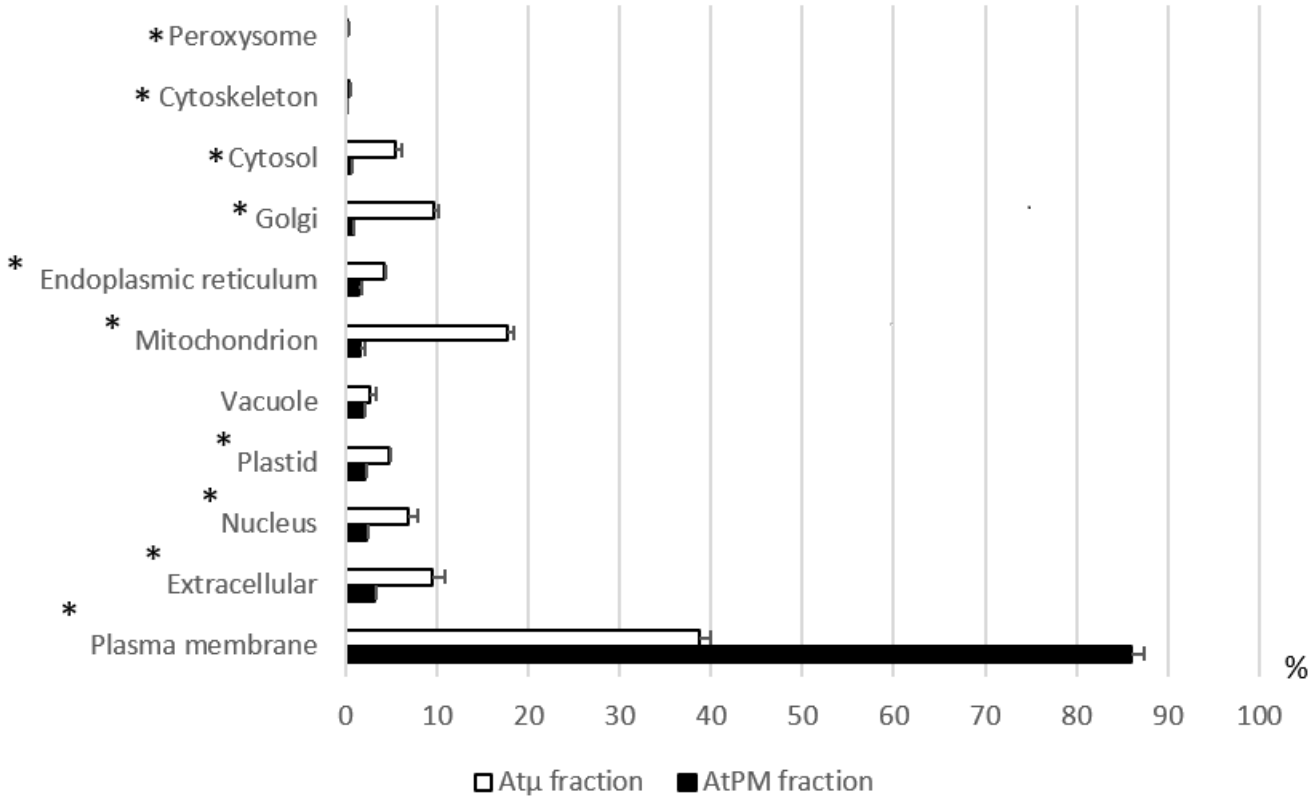
*Peroxysome
* Cytoskeleton
*Cytosol
* Golgi
* Endoplasmic reticulum
* Mitochondrion
Vacuole
* Plastid
* Nucleus
* Extracellular
* Plasma membrane
%
0
10
20
30
40
50
60
70
80
90
100
Atμ fraction
AtPM fraction

Figure 2

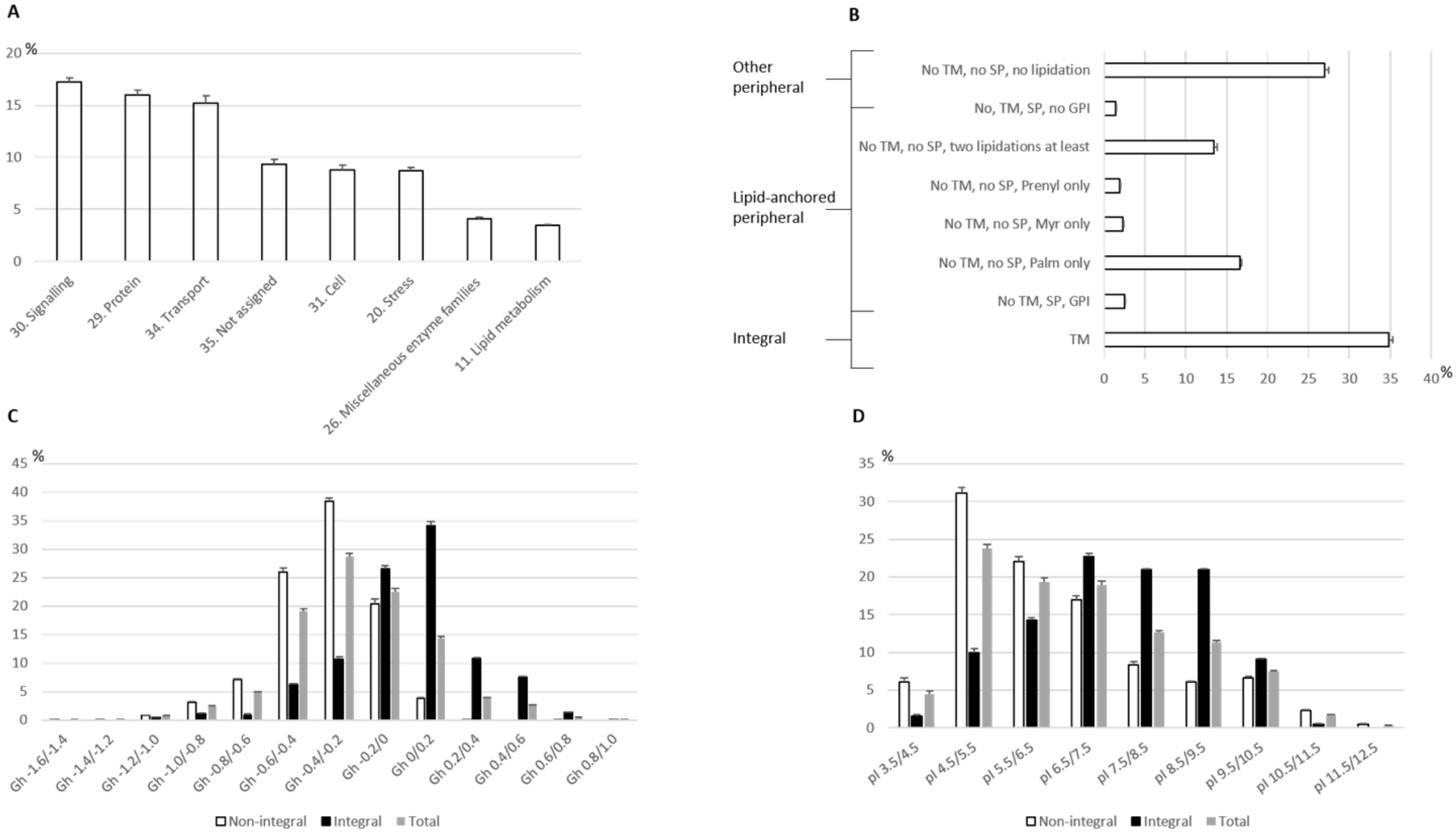
A
%
20
15
10
5
0
30. Signalling
29. Protein
34. Transport
35. Not assigned
31. Cell
20. Stress
26. Miscellaneous enzyme families
11. Lipid metabolism
B
Other peripheral
Lipid-anchored peripheral
Integral
No TM, no SP, no lipidation
No, TM, SP, no GPI
No TM, no SP, two lipidations at least
No TM, no SP, Prenyl only
No TM, no SP, Myr only
No TM, no SP, Palm only
No TM, SP, GPI
TM
0 5 10 15 20 25 30 35 40 %
C
%
45
40
35
30
25
20
15
10
5
0
Gh -1.6/-1.4
Gh -1.4/-1.2
Gh -1.2/-1.0
Gh -1.0/-0.8
Gh -0.8/-0.6
Gh -0.6/-0.4
Gh -0.4/-0.2
Gh -0.2/0
Gh 0/0.2
Gh 0.2/0.4
Gh 0.4/0.6
Gh 0.6/0.8
Gh 0.8/1.0
Non-integral
Integral
Total
D
%
35
30
25
20
15
10
5
0
pI 3.5/4.5
pI 4.5/5.5
pI 5.5/6.5
pI 6.5/7.5
pI 7.5/8.5
pI 8.5/9.5
pI 9.5/10.5
pI 10.5/11.5
pI 11.5/12.5
Non-integral
Integral
Total

Figure 3

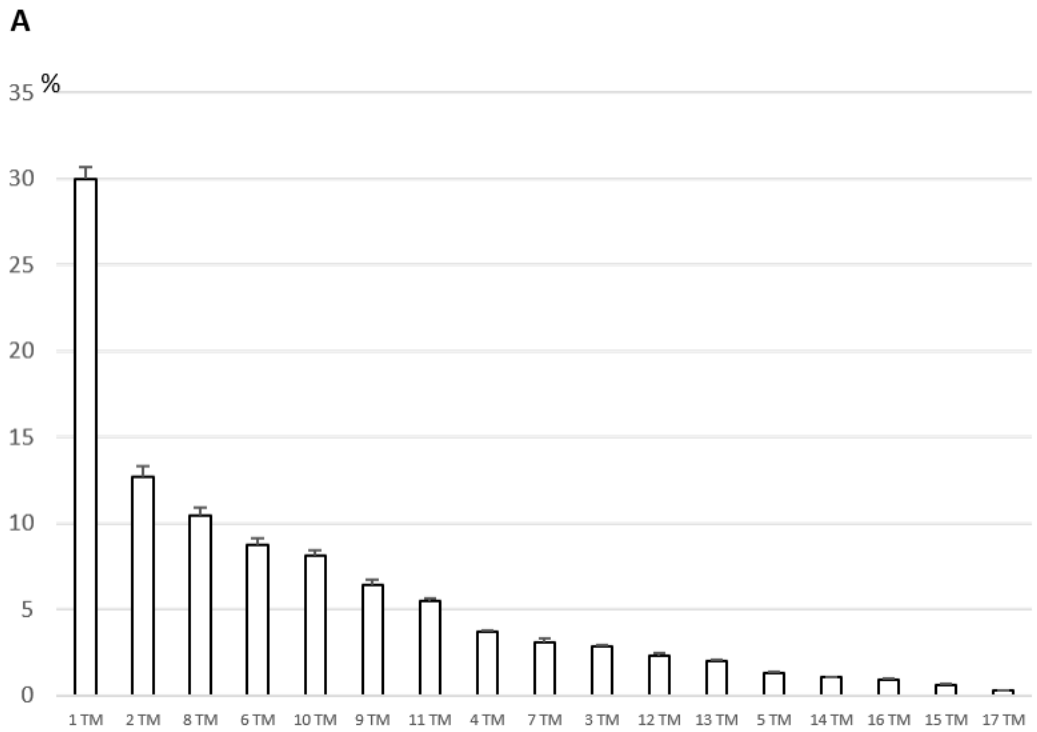
A
%
35
30
25
20
15
10
5
0
1 TM
2 TM
8 TM
6 TM
10 TM
9 TM
11 TM
4 TM
7 TM
3 TM
12 TM
13 TM
5 TM
14 TM
16 TM
15 TM
17 TM

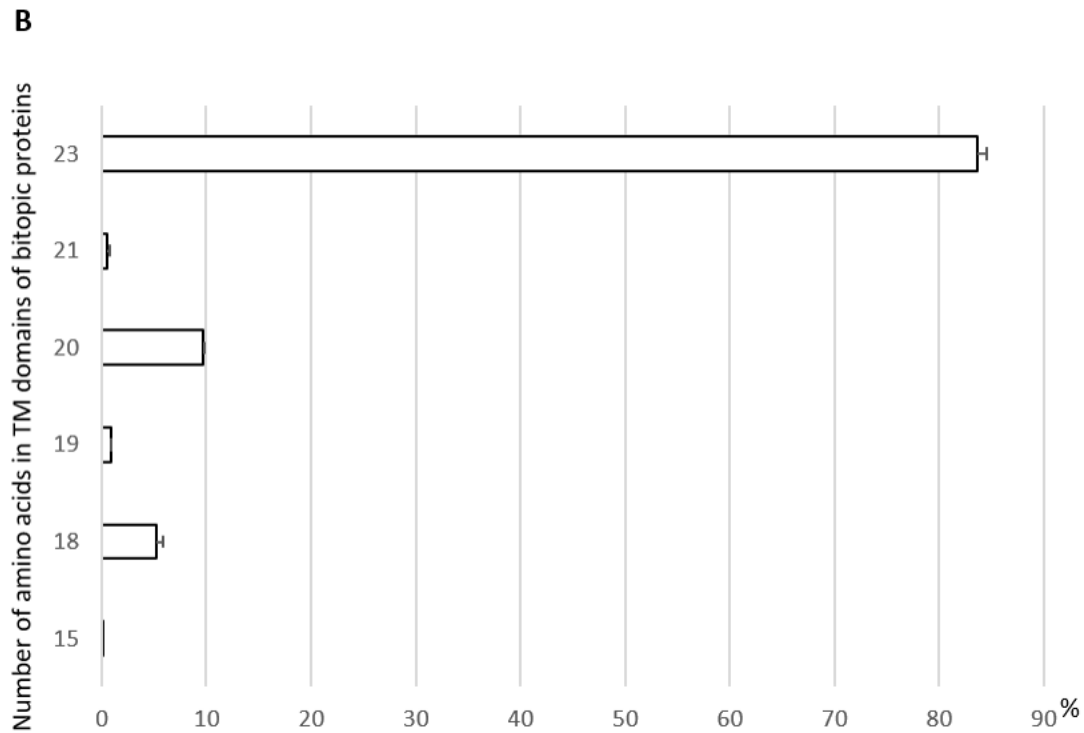
B
Number of amino acids in TM domains of bitopic proteins
23
21
20
19
18
15
0
10
20
30
40
50
60
70
80
90
%

Figure 4

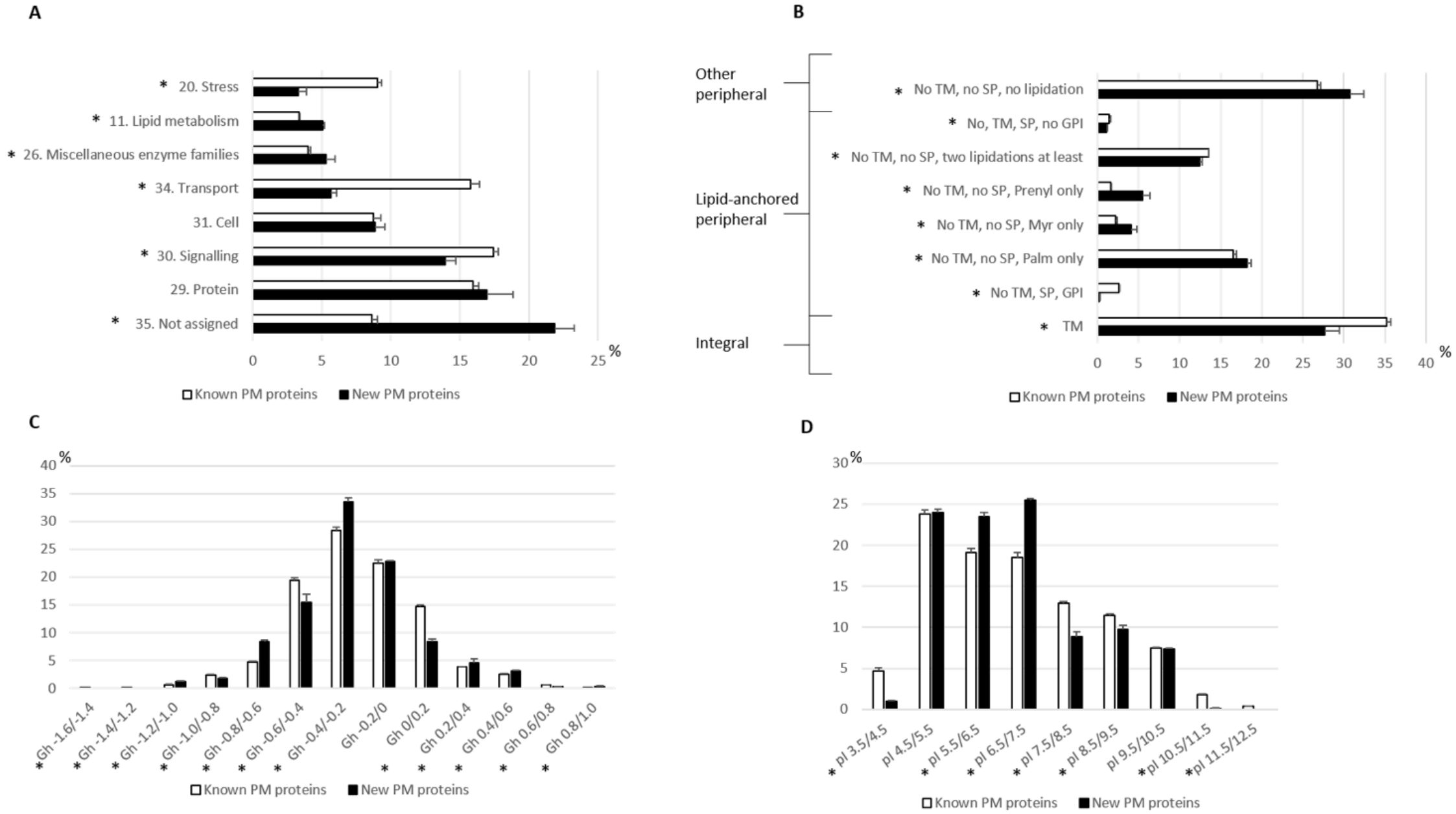
A
* 20. Stress
* 11. Lipid metabolism
* 26. Miscellaneous enzyme families
* 34. Transport
31. Cell
* 30. Signalling
29. Protein
* 35. Not assigned
0 5 10 15 20 25 %
Known PM proteins
New PM proteins
B
Other peripheral
Lipid-anchored peripheral
Integral
* No TM, no SP, no lipidation
* No, TM, SP, no GPI
* No TM, no SP, two lipidations at least
* No TM, no SP, Prenyl only
* No TM, no SP, Myr only
* No TM, no SP, Palm only
* No TM, SP, GPI
* TM
0 5 10 15 20 25 30 35 40 %
Known PM proteins
New PM proteins
C
40 %
35
30
25
20
15
10
5
0
* Gh -1.6/-1.4
* Gh -1.4/-1.2
* Gh -1.2/-1.0
* Gh -1.0/-0.8
* Gh -0.8/-0.6
* Gh -0.6/-0.4
* Gh -0.4/-0.2
Gh -0.2/0
* Gh 0/0.2
* Gh 0.2/0.4
* Gh 0.4/0.6
* Gh 0.6/0.8
* Gh 0.8/1.0
Known PM proteins
New PM proteins
D
30 %
25
20
15
10
5
0
* pI 3.5/4.5
pI 4.5/5.5
* pI 5.5/6.5
* pI 6.5/7.5
* pI 7.5/8.5
* pI 8.5/9.5
pI 9.5/10.5
* pI 10.5/11.5
* pI 11.5/12.5
Known PM proteins
New PM proteins

Figure 5

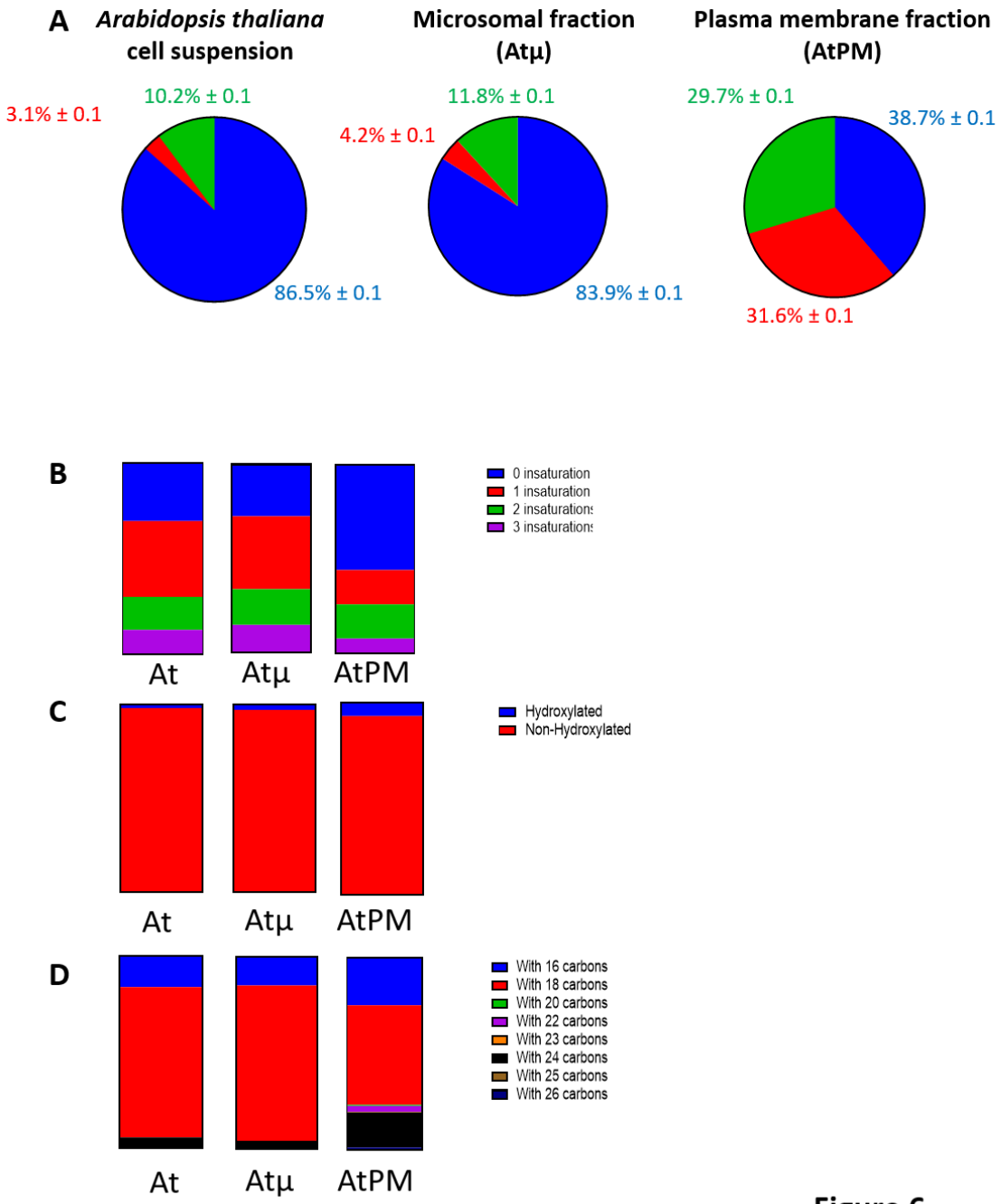
A
Arabidopsis thaliana cell suspension
3.1% ± 0.1
10.2% ± 0.1
86.5% ± 0.1
Microsomal fraction (Atμ)
4.2% ± 0.1
11.8% ± 0.1
83.9% ± 0.1
Plasma membrane fraction (AtPM)
29.7% ± 0.1
38.7% ± 0.1
31.6% ± 0.1
B
0 insaturation
1 insaturation
2 insaturations
3 insaturations
At
Atμ
AtPM
C
Hydroxylated
Non-Hydroxylated
At
Atμ
AtPM
D
With 16 carbons
With 18 carbons
With 20 carbons
With 22 carbons
With 23 carbons
With 24 carbons
With 25 carbons
With 26 carbons
At
Atμ
AtPM

Figure 6

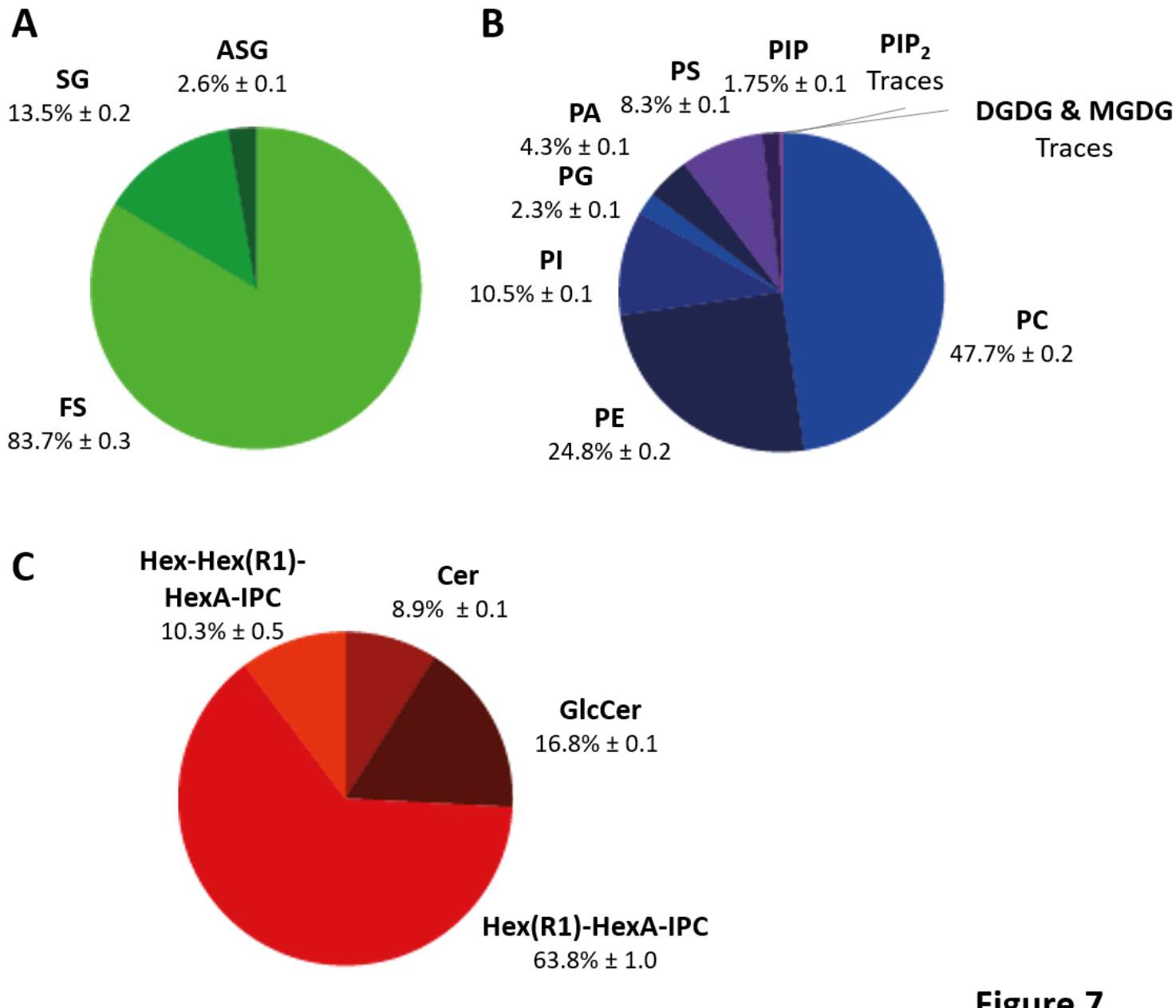
A
ASG
2.6% ± 0.1
SG
13.5% ± 0.2
FS
83.7% ± 0.3
B
PIP
1.75% ± 0.1
PIP2
Traces
PS
8.3% ± 0.1
PA
4.3% ± 0.1
DGDG & MGDG
Traces
PG
2.3% ± 0.1
PI
10.5% ± 0.1
PC
47.7% ± 0.2
PE
24.8% ± 0.2
C
Hex-Hex(R1)-
HexA-IPC
10.3% ± 0.5
Cer
8.9% ± 0.1
GlcCer
16.8% ± 0.1
Hex(R1)-HexA-IPC
63.8% ± 1.0

Figure 7

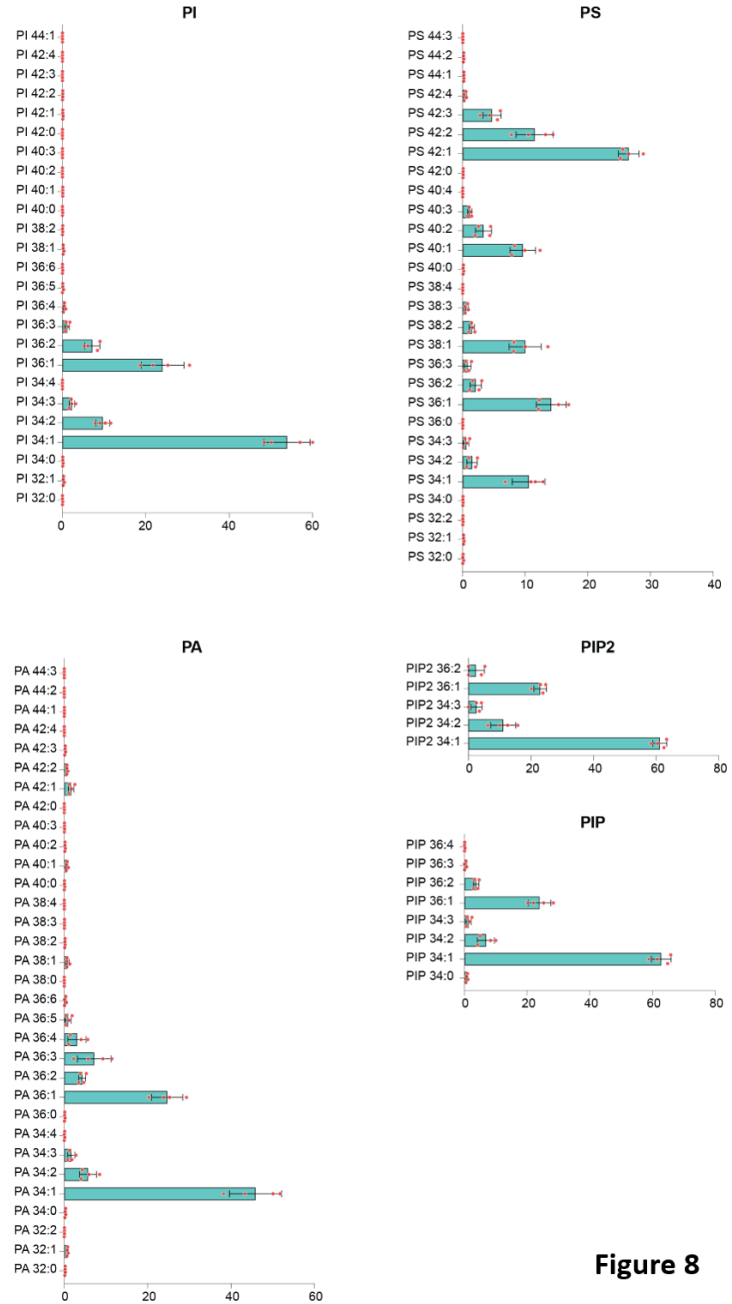
PI
PI 44:1
PI 42:4
PI 42:3
PI 42:2
PI 42:1
PI 42:0
PI 40:3
PI 40:2
PI 40:1
PI 40:0
PI 38:2
PI 38:1
PI 36:6
PI 36:5
PI 36:4
PI 36:3
PI 36:2
PI 36:1
PI 34:4
PI 34:3
PI 34:2
PI 34:1
PI 34:0
PI 32:1
PI 32:0
0
20
40
60
PS
PS 44:3
PS 44:2
PS 44:1
PS 42:4
PS 42:3
PS 42:2
PS 42:1
PS 42:0
PS 40:4
PS 40:3
PS 40:2
PS 40:1
PS 40:0
PS 38:4
PS 38:3
PS 38:2
PS 38:1
PS 36:3
PS 36:2
PS 36:1
PS 36:0
PS 34:3
PS 34:2
PS 34:1
PS 34:0
PS 32:2
PS 32:1
PS 32:0
0
10
20
30
40
PA
PA 44:3
PA 44:2
PA 44:1
PA 42:4
PA 42:3
PA 42:2
PA 42:1
PA 42:0
PA 40:3
PA 40:2
PA 40:1
PA 40:0
PA 38:4
PA 38:3
PA 38:2
PA 38:1
PA 38:0
PA 36:6
PA 36:5
PA 36:4
PA 36:3
PA 36:2
PA 36:1
PA 36:0
PA 34:4
PA 34:3
PA 34:2
PA 34:1
PA 34:0
PA 32:2
PA 32:1
PA 32:0
0
20
40
60
PIP2
PIP2 36:2
PIP2 36:1
PIP2 34:3
PIP2 34:2
PIP2 34:1
0
20
40
60
80
PIP
PIP 36:4
PIP 36:3
PIP 36:2
PIP 36:1
PIP 34:3
PIP 34:2
PIP 34:1
PIP 34:0
0
20
40
60
80

Figure 8

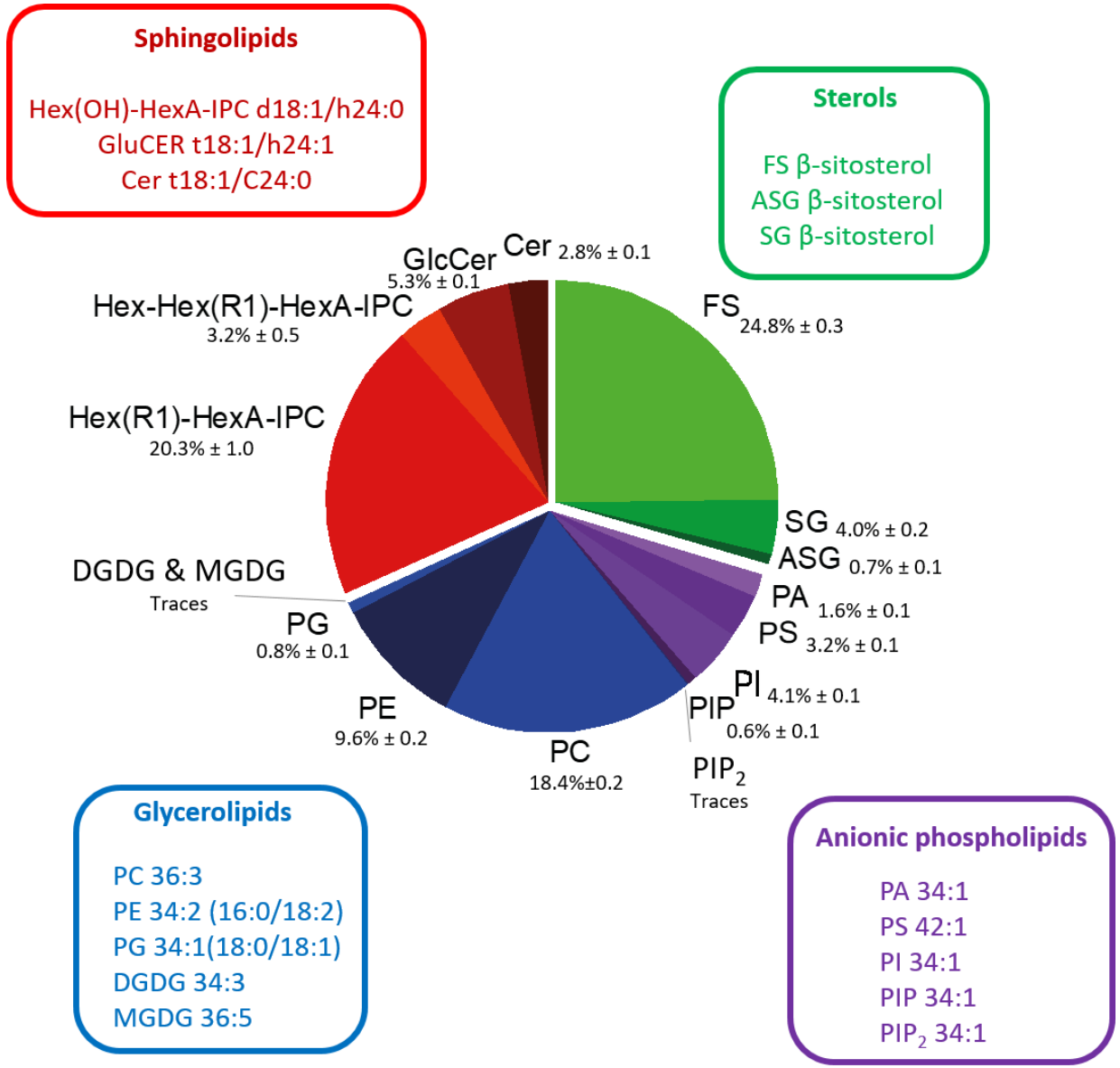
Sphingolipids
Hex(OH)-HexA-IPC d18:1/h24:0
GluCER t18:1/h24:1
Cer t18:1/C24:0
Sterols
FS β-sitosterol
ASG β-sitosterol
SG β-sitosterol
Cer 2.8% ± 0.1
GlcCer 5.3% ± 0.1
Hex-Hex(R1)-HexA-IPC 3.2% ± 0.5
Hex(R1)-HexA-IPC 20.3% ± 1.0
FS 24.8% ± 0.3
SG 4.0% ± 0.2
ASG 0.7% ± 0.1
PA 1.6% ± 0.1
PS 3.2% ± 0.1
PI 4.1% ± 0.1
PIP 0.6% ± 0.1
PIP2 Traces
PC 18.4%±0.2
PE 9.6% ± 0.2
PG 0.8% ± 0.1
DGDG & MGDG Traces
Glycerolipids
PC 36:3
PE 34:2 (16:0/18:2)
PG 34:1(18:0/18:1)
DGDG 34:3
MGDG 36:5
Anionic phospholipids
PA 34:1
PS 42:1
PI 34:1
PIP 34:1
PIP2 34:1

Figure 9